UNIVERSITEIT VAN PRETORIA
UNIVERSITY OF PRETORIA
YUNIBESITHI YA PRETORIA

COMPARISON OF FILTERED BACK PROJECTION AND OSEM IN REDUCING BLADDER ARTIFACTS IN PELVIC SPECT IMAGING

Agatha Katua

Thesis presented in partial fulfilment of the requirements for the Degree of Science in Medical Sciences (Nuclear Medicine) at the University of Pretoria

September 2010

© University of Pretoria

UNIVERSITEIT VAN PRETORIA
UNIVERSITY OF PRETORIA
YUNIBESITHI YA PRETORIA

DECLARATION

I, AGATHA MARY KATUA hereby declare that the work contained in this thesis is my own original work and has not previously in it's entirely or in part, been submitted at any university for a degree.

.....

Dr AGATHA MARY KATUA

..13...Day of. September 2010

Department of Nuclear Medicine

Steve Biko Academic Hospital

Faculty of Medicine

University of Pretoria

Copyright©2010 University of Pretoria

All Rights Reserved

DEDICATION

This thesis is dedicated to the Almighty God who always strengthens me.

TABLE OF CONTENTS

ACKNOWLEDGEMENTS

I gratefully acknowledge Professor Mike M Sathekge, the Head of the Department of Nuclear Medicine, Steve Biko Academic Hospital, and University of Pretoria, for his teaching support during my training in his department, and for his continued and tireless guidance through every step of carrying out the research and writing this thesis.

My gratitude extends to the consultants in the Department of Nuclear Medicine Steve Biko Academic Hospital, namely Drs P. Mpikashe, N. Mokgoro, N. Soni, W van Vuuren and N. Nyakale, and senior registrar Dr M Vorster for their valuable teaching and guidance.

My thanks also go to my colleagues and friends in the department, Dr A. Ankrah, T. Motshudi and D. Mshelia for their support and assistance.

I acknowledge the assistance of the Nuclear medicine technologists and all staff.

I thank Dr S Olorunju, biostatistician from Medical Research Centre for statistical advice.

I am grateful to my loving Mother, Eliwaza J Katua, who has been my role model for support, caring, grace and dignity, to my siblings for their love and support and to my adored children, Justina Wendy, Imelda Eliwaza and Joanne my love for them kept me going.

UNIVERSITEIT VAN PRETORIA
UNIVERSITY OF PRETORIA
YUNIBESITHI YA PRETORIA

SUMMARY

SUMMARY IN A MANUSCRIPT FORM SUBMITTED FOR PUBLICTION IN THE WJNM

Optimization of OSEM reconstruction in reducing bladder artifacts in SPECT imaging

*AM Katua, *AO Ankrah, *M Vorster, #A van Gelder, *MM Sathekge

* Department of Nuclear Medicine, University of Pretoria & Steve Biko Academic Hospital

Department of Internal Medicine Medicine, University of Pretoria & Steve Biko Academic Hospital

Summary

Bladder artifacts during bone single photon emission computed tomography (SPECT) is a common source of errors. The extent and severity of bladder artifacts have been described for filtered back projection (FBP) reconstruction. Ordered-subset expectation maximization (OSEM) may help to address this poor record of bladder artifacts, which render up to 20% of the images unreadable.

Aims and objectives

To evaluate the relationship of the bladder to acetabulum ratio in guiding the choice of the number of iterations and subsets used for OSEM reconstruction, for reducing bladder artifacts found on FBP reconstruction.

Materials and Methods

105 patients with various indications for bone scans were selected and planar and SPECT images were acquired. The SPECT images were reconstructed with both filtered back projection and OSEM using four different combinations of iterations and subsets. The images were given to three well experienced Nuclear Physicians who were blinded to the diagnosis and type of reconstruction used. They then labelled images from the best to the worst after which the data was analysed. The bladder to acetabulum ratio for each image was determined which was then correlated with the different iterations and subsets used.

Results

The study demonstrated that reconstruction using OSEM led to better lesion detectability compared to filtered back projection in 87.62% of cases. It further demonstrated that the iterations and subsets used for reconstruction of an image correlates to the bladder to acetabulum ratio. Four iterations and 8 subsets yielded the best results in 48.50% of the images whilst two iterations and 8 subsets yielded the best results in 33.80%. The number of reconstructed images which yielded the best results with 2 iterations and 8 subsets were the same as or more than those with 4 iterations and 8 subsets when the bladder/acetabulum ratio was between 0.20-0.39. A ratio below 0.20 or above 0.39 supports the usage of 4 iterations and 8 subsets over 2 iterations and 8 subsets.

Conclusion

Bladder to acetabulum ratio can be used to select the optimum number of iterations and subsets for reconstruction of bone SPECT for accurate characterization of lesions.

This study also confirms that reconstruction with OSEM (vs FBP) leads to better lesion detectability and characterisation.

Introduction

Bone imaging of the pelvis is an important diagnostic test for the detection of avascular necrosis of the femoral heads, for the detection of metastatic tumors and other diseases such as osteomyelitis. Although planar imaging is possible, single photon emission computed tomography (SPECT) offers improved sensitivity and specificity due to its greater contrast and ability to differentiate overlying internal structures. With the availability of SPECT the sensitivity of avascular necrosis detection for example, has been shown to be 85%, compared to 55% for planar imaging, with no loss of specificity.

However, bladder artifacts during bone SPECT is a common source of errors. The extent and severity of bladder artifacts have been well described for filtered back projection (FBP) reconstruction. Ordered-subset expectation maximization (OSEM) may help to address this poor record of bladder artifacts, which render up to 20% of the images unreadable [(1)].

Accurate and reliable lesion detectability on images is important to guide therapeutic management, improve risk stratification, and provide prognostic information in the pelvic evaluation of patients. Hence it is crucial that the results are reliable and reproducible. The performances of OSEM and FBP have been compared in a number of other experimental and clinical studies, with a variety of reconstruction parameters employed with OSEM as well as the use of post reconstruction smoothing to replace noise with increasing number of iterations. To date no consensuses have been reached. [(2-6)]

Whilst previous studies have demonstrated better lesion detectability with attenuation correction, OSEM and dynamic expectation maximum, none of these studies has determined the ideal number of iterations and subsets for any given patient or any given condition. The large number of combinations of iterations and subsets in OSEM may discourage the use of OSEM in the clinical setting. Again since the patient from whom these images are acquired have different physiological and pathological processes which would alter the rate of tracer excretion, extraction of tracer by bone and bone to soft tissue ratio. It is important that a practical simple and reproducible way of determining the best iteration and subset to use for each patient which would take into account the activity of the tracer activity in the bladder and the uptake by

bone. The hip and the bladder activity (the cause of the artifacts) are easily identifiable on the whole body scan and a ratio of the counts from these provides a good individualized index against which iterations and subsets of OSEM used for reconstruction can be optimized.

Blocklet et al noted that 2 iterations and 8 subsets gave acceptable iterations for most images [(2)]. Case et al also used 12 by 3 subsets and iterations [(3)]. Number of subsets and iterations will further be referred to as (subset X iterations) that is (12x3).

Materials and Methods

This was a prospective study which included 105 adult patients; 59 female and 46 male *(See Table 1)* who were routinely referred for bone scintigraphy to the Department of Nuclear Medicine, University of Pretoria between October 2008 and March 2009. The inclusion- and exclusion criteria used are contained in Table 2.

Ethics approval was obtained from the Faculty of Health Sciences Research Ethics Committee, University of Pretoria and informed written consent was obtained from all study participants.

Table 1: Demographics of Study Population

Demographics of study population		
Gender	59 female	46 male
Age	Avg 55 (+/-14.6)	Avg 55 (+/-17)

Table 2: Inclusion and Exclusion Criteria

Inclusion Criteria	Exclusion Criteria
All adult patients routinely referred for bone scintigraphy with equivocal pelvic lesions on planar images.	Pregnancy and breastfeeding
	Dehydrated patients
	Patients on whom pelvic SPECT is impossible due to poor patient cooperation.

Patients were referred for various indications and we selected those where the primary region of interest was the pelvis or instances where pelvic lesions on planar images could not be confidently characterized in the absence of SPECT imaging. Images were processed and analyzed (as demonstrated in Fig 1).

105 patients consented to the study however 25 were lost because their SPECT images were incomplete or lost.

Data Analysis Flow chart

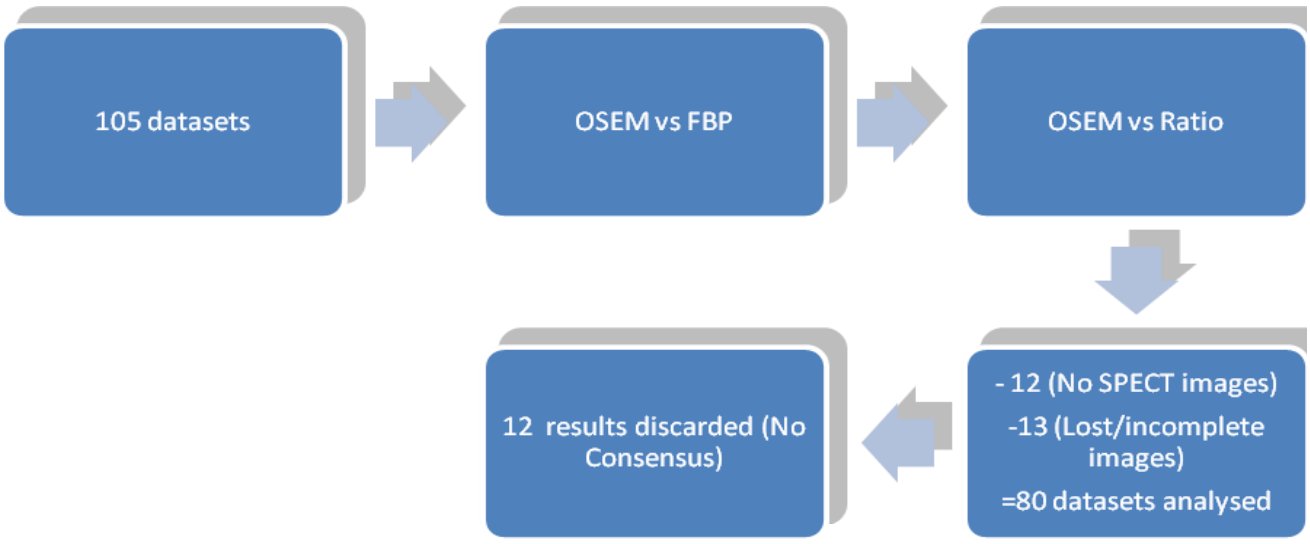

Fig 1

The standard departmental imaging protocol was followed for each patient (adapted from current SNM and EANM guidelines) starting with the acquisition of whole body planar/ spot images and proceeding to SPECT image acquisition where needed [7,8] *(See Fig 2)*

The SPECT images were reconstructed with both filtered back projection and OSEM using four different combinations of (subset x iterations). These were 2x8, 4x8, 3x12 and 6x12. *(See Fig 3)*

FBP reconstruction was done with a Butterworth filter at 0.5 of Nyquist frequency and OSEM iterative reconstruction with various combinations of iterations and subsets.
With OSEM reconstruction a non-negativity constraint was applied, which meant that negative line of response values (because of random correction)

and negative pixel values were set to zero. Limitations in terms of the number of subsets (nine different subsets) and iterations (limited to 30) programmed in the OSEM reconstruction, was a restriction encountered during reconstructions. For OSEM with a subset size of 1, the number of iterations required to achieve good image quality is typically 30–50, but there is no clear guidance or recommendation for an appropriate combination [9]

Hence a new suggestion of introducing a relationship with acetabulum/bladder (A/B) ratio as means of choosing an appropriate subset size which permits a more complete evaluation of the effect of the number of iterations on image noise and artifact. This could be a reliable and repeatable method if validated.

For this A/B a line profile across the acetabulum and the bladder was drawn and compared to OSEM performance.

The images were given to three well experienced Nuclear Physicians who were blinded to the type of reconstruction used. They then labelled images from the best to the worst after which the data was analysed. The acetabulum to bladder ratio for each image was determined which was then correlated with the different (subset x iterations) used.

Table 3: Assessment Scale

Grade 1	Non-diagnostic image	
Grade 2	Poor quality image	L:B <1
Grade 3	Adequate quality	L:B =1
Grade 4	Good quality Image	L:B >1

Images were assessed on a 4-point scale *(See Table 3)* for the presence of artifacts and the clinical impact of artifacts on diagnosis of pelvic abnormalities.

A blind analysis technique was used in an attempt to eliminate bias, whereby the FBP result was hidden from the analysts until reviewers agreed—based on properties of the data set from OSEM.

Correlation analysis was performed between acetabulum bladder ratio and various OSEM reconstruction parameters and p-values less than 0.05 were considered significant.

Results

105 patient 56% females and 44% males were studied. The average age was 55years with a standard deviation of 15 years. It was observed that out of the 105 images reconstructed using FBP reconstruction method; only 13 images were rated as grade 4 in comparison to those which were reconstructed using OSEM reconstruction method (12.4%). The remaining 92 images reconstructed using OSEM method of reconstruction images were rated as grade 4 (87.62%) *(See Fig.3).* Reconstruction of imaging using OSEM led to better lesion detectability compared to filtered back projection in **87.6%** of cases. It further demonstrated that the (subset x iterations) used for reconstruction of an image correlates with the (A/B) ratio. (4 x 8) yielded the best results in **48.5%** of the images whilst (2 x 8) yielded the best results in **33.8%.** The number of reconstructed images which yielded the best results with (2 x 8) was the same as or more than those with (4 x 8) when the (A/B) ratio was between 0.20-0.39. A ratio below 0.20 or above 0.39 supported the use of (4 x 8) over (2 x 8). Although less common, should the ratio be above 0.69, then (3 x12) will provide image qualities of grade 3 & 4.*(See Table 4 and Results Graph, Fig 5)*

In reconstructed images OSEM reconstruction method led to a significant reduction in bladder artifacts when compared to FBP reconstruction method. Images reconstructed using FBP method of reconstruction completely differs from images reconstructed using OSEM method of reconstruction.

Compared to FBP the OSEM method of reconstruction significantly reduced ($p = 0.0001$) the bladder artifact in the pelvis in SPECT imaging. It improved the uniformity and symmetry of bone tracer-uptake, and thus optimized lesion detectability. The reduction of pelvic bladder artifacts in the OSEM reconstructed images was independent of diagnosis, age or gender of the patients.

A: FBP

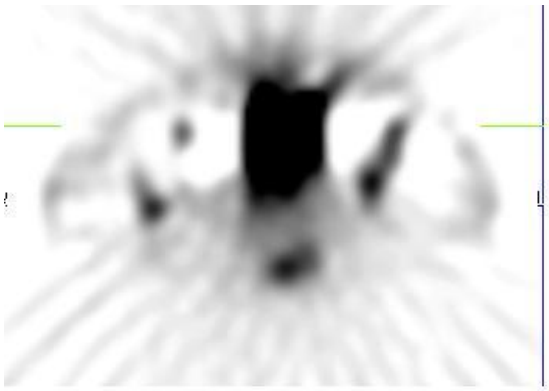

B: OSEM 2x8

C: OSEM: 4x8

D: OSEM: 3x12

Fig 2: A-D

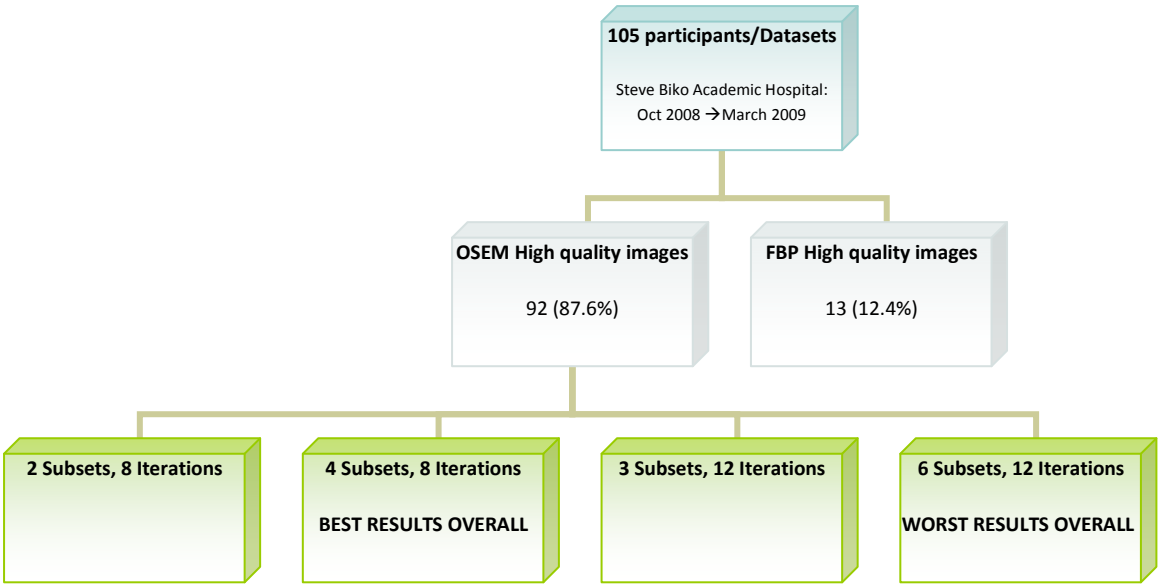
105 participants/Datasets
Steve Biko Academic Hospital:
Oct 2008 → March 2009
OSEM High quality images
92 (87.6%)
FBP High quality images
13 (12.4%)
2 Subsets, 8 Iterations
4 Subsets, 8 Iterations
BEST RESULTS OVERALL
3 Subsets, 12 Iterations
6 Subsets, 12 Iterations
WORST RESULTS OVERALL

Fig 3

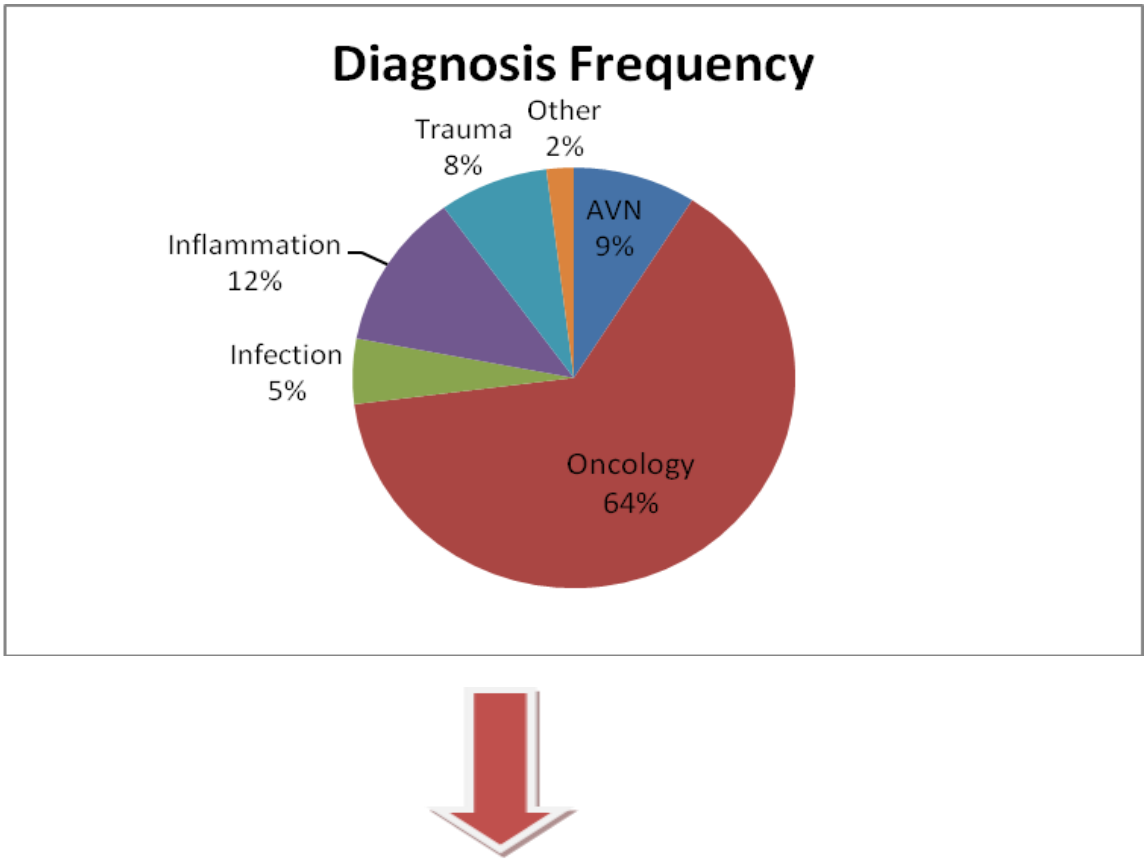
Diagnosis Frequency
Trauma 8%
Other 2%
AVN 9%
Inflammation 12%
Infection 5%
Oncology 64%

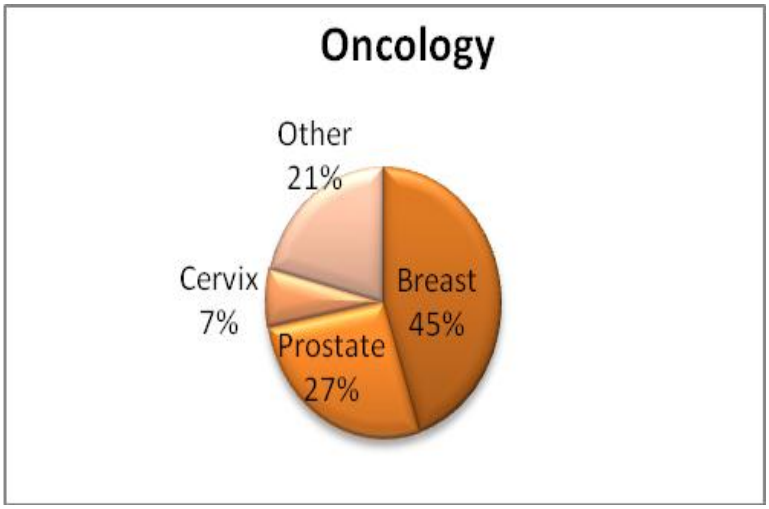

Fig 4

Oncology-related referrals made up the majority of our study population (64%) with the most prevalent cancers being breast (45%) and prostate (27%). Inflammation, Avascular necrosis of the head of the femur (AVN) and trauma-related indications were the next most common reasons for referral.

Table 4: Correlation of various subset x iterations combinations with Acetabulum/Bladder ratio in Percentage

	No of images rated as best (%)
4x8	33 (48.53)
2x8	23 (33.82)
3x12	10 (14.71)
6x12	2 (2.94)

Acetabulum/Bladder Ratio vs. Iterations x Subsets

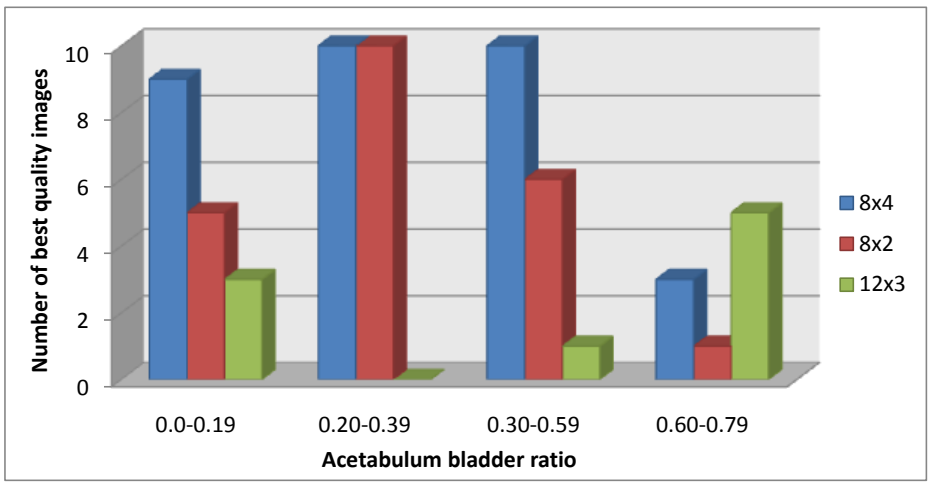

Fig 5

Discussion

SPECT imaging of the pelvis has been well established as an important diagnostic test for various indications. These include AVN of the femoral heads, localization in various metastatic tumours and osteomyelitis of the hips amongst others.

However, two important confounding issues frequently limit the accuracy of pelvic bone SPECT, leading to both false positives and false negatives.

Firstly, the attenuation of emitted activity due to non-homogenous attenuation distribution may result in inconsistent projection measurements of the radiotracer distribution. As a result of these inconsistent measurements, it is possible for streaking artifacts to appear in reconstructed images, which may reduce lesion contrast within the pelvic region [(1)]. This effect may be reduced by acquiring transmission measurements using an external radioactive source

and incorporating attenuation compensation into the image reconstruction process.

Secondly, during pelvic SPECT acquisition, inconsistent projection data is acquired as a result of accumulation of activity into the bladder during the data acquisition process. When reconstructed with conventional image reconstruction procedures such as FBP, image artifacts will appear as streaks through the bladder region [10]. The extent of these streaks is dependent upon both the amount of activity accumulating in the bladder as well as on the rate of uptake of activity into the bladder. When either the amount or rate of uptake is not significant, these streaks will not appear significant. In many cases however, the amount and/or rate of uptake is significant and produce streak artifacts. Bladder artefacts may also be a result from scattered counts that are mis-positioned in the image due to Compton scatter. A further study can be done to investigate the role of a scatter correction in conjunction with the OSEM reconstruction to see how the images will improve. It should be noted out that attenuation consist of photon absorption as well as Compton scatter. Compton scatter not corrected for may result in inappropriate attenuation corrections being applied. Scattered photons originating from the bladder can also result in artifacts being created in the skeletal areas.

The above-mentioned artifacts may mask other regions within the pelvis, thus possibly reducing lesion detection. They can appear as anomalous blobs of apparent activity, which may be mistaken for tumors (false positives), or as dark shadows, which can hide true lesions (false negatives) [6, 10] and mimic the photon-deficient regions of avascular necrosis [11]. The bladder-filling artifacts that occur in pelvic imaging are particularly severe, rendering as many as 20% of SPECT scans of this region unusable [1].

The following has been suggested as possible solutions:

Attenuation correction (AC) has been shown to improve bone SPECT image quality in other regions of the body, such as the cervical spine [3] and to improve lesion detection in thoracic SPECT [6]. PET images of the pelvis have also been shown to benefit from AC [12]. Unfortunately, AC alone may not be sufficient for pelvic SPECT, because changing activity in the bladder throughout the acquisition contributes to the artifact. Catheterization is a possible means

of mediating this effect but it has an associated increased risk of complications such as infection and consequently is unattractive for general application.

FBP vs. OSEM

FBP has been the standard technique for tomographic image reconstruction in clinical nuclear medicine. However, FBP can result in the generation of artefacts, which mainly consist of streaking and negative counts near the borders of hot objects [11, 13]. There are myriad iterative reconstruction algorithms that can be used as alternative reconstruction techniques to FBP. However, many of these, such as maximum likelihood expectation maximization (MLEM), are computationally intensive and have never been used in clinical practice [14]. Various methods have been developed to accelerate the speed of these algorithms. The most widely used acceleration technique is the ordered subset procedure of Hudson and Larkin [9], which resulted in the development of the OSEM technique. The OSEM algorithm recently has become available on many commercial nuclear medicine computer systems and is now being used in routine clinical practice [2, 15].

Bladder artifacts in pelvic SPECT are known to be caused by the non-uniform attenuating media and changing bladder activity [11], both of which also lead to incomplete cancellation of side lobes in FBP, and so iterative reconstruction would be expected to reduce the magnitude of the artifact. With the availability of faster hardware and more efficient iterative reconstruction techniques, algorithms such as OSEM are now moving from the research environment into routine clinical use. It is important to understand the quality control requirements that such algorithms place on imaging systems.

Whilst iterative methods of reconstruction have gained wide clinical acceptability in relatively newer nuclear medicine techniques such as PET its use for the relatively older procedures has not gained wide clinical acceptability. The numerous amounts of iterative and subsets one must use to get an optimum image interrupts the usual work flow in busy nuclear medicine department. An index that would reduce the number of trials of reconstruction would provide an acceptable method and probable encourage the use of OSEM in clinical bone SPECT. This study revealed that for bladder acetabulum ratios less than 0.59 the best images would be produced by (4 x 8) as the ratio increases a higher number of iterations (3 x 12). The improvement at higher level is however lost at higher iterations and subsets because it accentuates the noise compromising the quality of the images as noted with (6 x 12).

Many comparison studies showed that iterative reconstruction outperforms FBP in terms of image quality, signal-to-noise ratio, resolution and contrast [23] and improves lesion detection. [24] It has been highlighted that the characteristics of the reconstructed images are bound to the chosen number of iterations and to the source distribution [25]. Convergence studies showed that the optimal number of iterations depends on the statistics of the input scan. The higher the statistics, the higher the number of iterations is to be used. In previous studies, determining the number of iterations and subsets enabling the most accurate parameter estimation was never validated [26]. The optimal number of MLEM equivalent updates (iterations x subsets) is object dependent and convergence does not occur at the same iteration for the whole image. The finding of the most appropriate parameters is even more complicated for bladder artifacts.

In this study, it was found that OSEM show a clear advantage in the quality of the reconstructed image, and a concern over the price paid in reconstruction time which may introduce delays into the daily work flow is no longer applicable due to new generation soft wares.

Importantly, this study is the first to report on a relationship between acetabulum bladder ratio and the choice of the number of iterations and subsets used for OSEM reconstruction. Hence the huge potential to reduce the reconstruction time by selecting either 2 iterations and 8 subsets or 4 iterations and 8 subsets when the bladder acetabulum is between 0.2-0.39. Four iterations and 8 subsets should be used if the ratio is below 0.2 or above 0.39. If confirmed by other authors, this methodology would also help in addressing the issue of reproducibility and reliability in follow-up studies. This can be thus be standardized by vendors on various work stations. To overcome the reconstruction dilemma, the installation of faster hardware, or use of a large subset size (between 4 and 8) to speed up the reconstruction [27] and reduce processing time will also be of benefit.

These requirements are well known for FBP, and some work is to be done to determine the uniformity requirements for algorithms such as OSEM. It has been reported previously that, in clinical practice, the use of iterative reconstruction techniques in place of FBP does not appear to alter the basic requirements for good gamma camera uniformity. However, the accuracy and validity of this information has not been critically examined as the results were

obtained from limited data using a subset size of one and 40 iterations were set at 40 (in OSEM reconstruction method) [27].

The current study also did not critically analyze the uniformity requirements for the reconstructed methods used having fixed the pixel size and the amount of post reconstruction filtering.

Despite the diversity in diagnosis, images reconstructed with OSEM method of reconstruction showed the best reduction of pelvic bladder artifacts, irrespective of the age or gender of the patients, when compared to images reconstructed with FBP method of reconstruction. In cases where avascular necrosis of the head of femur is suspected, very high resolution planar images of the region (acquired using a pinhole collimator) have an advantage over SPECT pelvic images reconstructed using OSEM. In some cases, a simple additional delayed (6 – 24hrs) planar image may result in higher target to background ratio, and permit better evaluation of the pelvis if it was obscured by the bladder, thus excluding the need for pelvic SPECT imaging. Hence, the results obtained are restricted to comparing the FBP and OSEM methods of reconstruction in reducing bladder artifacts, when SPECT pelvic imaging is necessary for accurate localization and detection of lesion.

To conclude, the bladder-filling artifact was significantly reduced in most patients and subjective evaluation of image quality demonstrated a significant difference between OSEM and FBP. Importantly, our study is the first to demonstrate the relationship of the bladder to acetabulum ratio in guiding the choice of the number of iterations and subsets used for reconstruction, which is most likely to lead to accurate lesion localisation and or characterisation.

References

1. Collier B, Carrera G, Johnson R, et al. Detection of femoral head avascular necrosis in adults by SPECT. J Nucl Med. 1985; 26:979–987.

2. Blocklet D, Seret A, Popa N, Schoutens A, Maximum likelihood reconstruction with ordered subsets in bone SPECT. J Nucl Med 1999; 40: 1978 – 1984

3. Case JA, Licho K, King MA, Weaver JP, Bone SPECT of the spine: a comparison of attenuation correction techniques. J Nucl Med 1999, 40: 604 – 613

4. Kauppinen T, Koskinen MO, Alenius S, Vanninen E, Kuikka JT, Improvement of brain perfusion SPET using iterative reconstruction with scatter and non – uniform attenuation correction, Eur J Nucl Med 2000, 27: 1380 – 1386

5. Vanhove C, Defrise M, Frankers PR, Evernert H, Deconinck F, Bossyut A, Interest of the ordered subsets expectation maximization (OSEM) algorithm in pinhole single-photon emission tomography reconstruction: a phantom study. Eur J Nucl Med 2000, 27: 140 – 146.

6. Wells GR, King MA, Simkin PH, Judy PF, Brill AB, Gifford HC et al. Comparing filtered back projection and ordered subsets expectation maximization for small- lesions detection and localization in 67Ga SPECT. J Nucl Med 2000, 41: 1391 – 1399.

7. Donohoe KJ, Henkin RE, Royal HD, Brown ML, Collier BD, O'Mara RE, Carretta RF. Procedure guideline for bone scintigraphy. Society of Nuclear Medicine. J Nucl Med 1996; 37: 1903-6.

8. Bombardieri E, Aktolun C, Baum RP, Bishof-Delaloye A, Buscombe J, Chatal JF, Maffioli L, Moncayo R, Mortelmans L, Reske SN. Bone Scintigraphy: Procedure Guideline for Tumour Imaging. Eur J Nucl Med Mol Imaging 2003; 30: BP99-106.

9. Hudson HM, Larkin RS. Accelerated image reconstruction using ordered subsets of projection data. IEEE Trans Med Imaging 1994;13:601.–609

10. King MA, Tsui BMW, Pan TS, Glick SJ, Soares EJ. Attenuation compensation for cardiac single-photon emission computed tomographic imaging: Part 2. Attenuation compensation algorithms. J Nucl Cardiol. 1996;3:55–63

11. Gillen G, McKillop J, Hilditch T, Davidson J, Elliot A. Digital filtering of the bladder in SPECT bone studies of the pelvis. J Nucl Med. 1988; 29:1587–1595

12. Turkington T, Coleman R. Effects of reconstruction methods and attenuation correction on hot bladder artifacts in PET [abstract]. J Nucl Med. 2000; 41(suppl): 194P.

13. Forstrom LA, Dunn WL, O'Connor MK, et al. Technical pitfalls in image acquisition, processing and display. Semin Nucl Med 1996; 26:278. –294.

14. Hutton BF, Hudson HM, Beekman FJ. A clinical perspective of accelerated statistical reconstruction. Eur J Nucl Med 1997; 24:797. –808.

15. Alush DS, Tsui BM. Performance of ordered-subset reconstruction algorithms under conditions of extreme attenuation and truncation in myocardial SPECT. J Nucl Med 2000; 41:737. –44

16. Bouchareb, K. Thielemans, T. Spinks, O. Rimoldi and P.G. Camici, Comparison of analytic and iterative reconstruction methods for quantitative cardiac PET studies in 3D using Oxygen-15 water scans, IEEE Nucl. Sci. Symp. Conf. Rec. 4 (2005), pp. 2120–2123.

17. Lartizien C, Kinahan PE, Swensson R, Comtat C, Lin M, Villemagne V and Trébossen R. Evaluating image reconstruction methods for tumor detection in 3-dimensional whole-body PET oncology imaging, J. Nucl. Med. 4 (2) (2003), pp. 276–290 (Feb.).

18. Gutman F, Gardin I, Delahaye N, Rakotonirina H, Hitzel A, Manrique A, Guludec DL and Véra P. Optimisation of the OS-EM algorithm and comparison with FBP for image reconstruction on a dual-head camera: a phantom and a clinical 18F-FDG study, Eur. J. Nucl. Med. Mol. Imaging 30 (11) (2003), pp. 1510–1519 (Nov.)

19. Reilhac A, Tomeï S, Buvat I, Michel C, Keheren F, Costes N. Simulation-based evaluation of OSEM iterative reconstruction methods in dynamic brain PET studies. Neuroimage. 2008 Jan 1; 39(1):359-68.

20. Leong LK, Kruger RL, O'Connor MK. A Comparison of the Uniformity Requirements for SPECT Image Reconstruction Using FBP and OSEM Techniques. J Nucl Med Technol 2001; 29:79-83

CHAPTER 1

INTRODUCTION

The basic principle of nuclear medicine imaging is the following: a γ-emitter–labelled pharmaceutical is administered to a subject and an external device, the gamma camera, detects the radioactivity stemming from the body, from 1 or several angles of views. The image obtained at 1 angle of view is the projection of the 3-dimensional (3D) distribution onto the 2-dimensional (2D) detector plane. Because of the projection operation, no information regarding the depth at which disintegrations occur is available; moreover, activities stemming from separate structures may overlap each other on the detector plane, and the contrast may be low. With only 1 projection image, it is impossible to determine the activity distribution because an infinite number of distributions can yield the same projection. It is as difficult as to find 2 values knowing only their sum. However, the overlap observed in the projections depends on the relative positions of the detector and of the structures inside the body. So, more information about the relative positions can be obtained by acquiring projections over a large number of angles of view around the subject.

The basic idea of Single Photon Emission Computed Tomography (SPECT) is to obtain, as accurately as possible, an image of the γ-emitter distribution in any slice of the body, using projections of this image acquired by a rotating gamma camera from several angles of view.

SPECT allows us to visualize functional information about a patient's specific organ or body system. SPECT manage to give us functional information happening in the body. Internal radiation is administered by means of a pharmaceutical which is labelled with a radioactive isotope. This so called radiopharmaceutical, or tracer, is injected, ingested, or inhaled. The radioactive isotope decays, resulting in the emission of gamma rays. These gamma rays give us a picture of what's happening inside the patient's body. By using the gamma camera gamma rays allow us to see inside. The gamma camera can be used in planar imaging to acquire 2-dimensional images, or in SPECT imaging to acquire 3-dimensional images. The gamma camera collects gamma rays that are emitted from within the patient, enabling us to reconstruct a picture of where the gamma rays originated. From this, we can determine how a particular organ or system is functioning.

The Gamma Camera

Once a radiopharmaceutical has been administered, it is necessary to detect the gamma ray emissions in order to attain the functional information. The

instrument used in Nuclear Medicine for the detection of gamma rays is known as the Gamma camera. The components making up the gamma camera are the collimator, detector crystal, photomultiplier tube array, position logic circuits, and the data analysis computer.

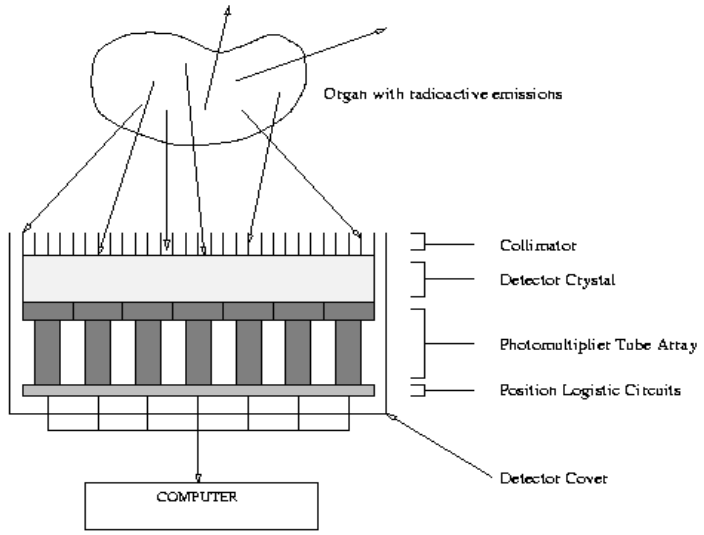

Fig.1: The Gamma Camera

1. Camera Collimator

The first object that an emitted gamma photon encounters after exiting the body is the collimator. The collimator is a pattern of holes through gamma ray absorbing material, usually lead or tungsten that allows the projection of the gamma ray image onto the detector crystal. The collimator achieves this by only allowing those gamma rays travelling along certain directions to reach the detector; this ensures that the position on the detector accurately depicts the originating location of the gamma ray.

2. Scintillation Detector

In order to detect the gamma photon we use scintillation detectors. A Thallium-activated Sodium Iodide [NaI(Tl)] detector crystal is generally used in Gamma cameras. This is due to this crystal's optimal detection efficiency for the gamma ray energies of radionuclide emission common to Nuclear Medicine. A detector crystal may be circular or rectangular. It is typically 9mm thick and has dimensions of 30-50 cm. A gamma ray photon interacts with the detector by means of the Photoelectric Effect or Compton Scattering with the iodide ions of the crystal. This interaction causes the release of electrons which in turn interact with the crystal lattice to produce light, in a process known as scintillation.

3. Photomultiplier Tubes

Only a very small amount of light is given off from the scintillation detector. Therefore, photomultiplier tubes are attached to the back of the crystal. At the face of a photomultiplier tube (PMT) is a photocathode which, when stimulated by light photons, ejects electrons. The PMT is an instrument that detects and amplifies the electrons that are produced by the photocathode. For every 7 to 10 photons incident on the photocathode, only one electron is generated. This electron from the cathode is focused on a dynode which

absorbs this electron and re-emits many more electrons (usually 6 to 10). These new electrons are focused on the next dynode and the process is repeated over and over in an array of dynodes. The dynodes are kept at an increasingly higher potential, this is the cause for the acceleration of the electrons from the one dynode to the next, which results in more electrons to be released at each dynode. At the base of the photomultiplier tube is an anode which attracts the final large cluster of electrons and converts them into an electrical pulse.

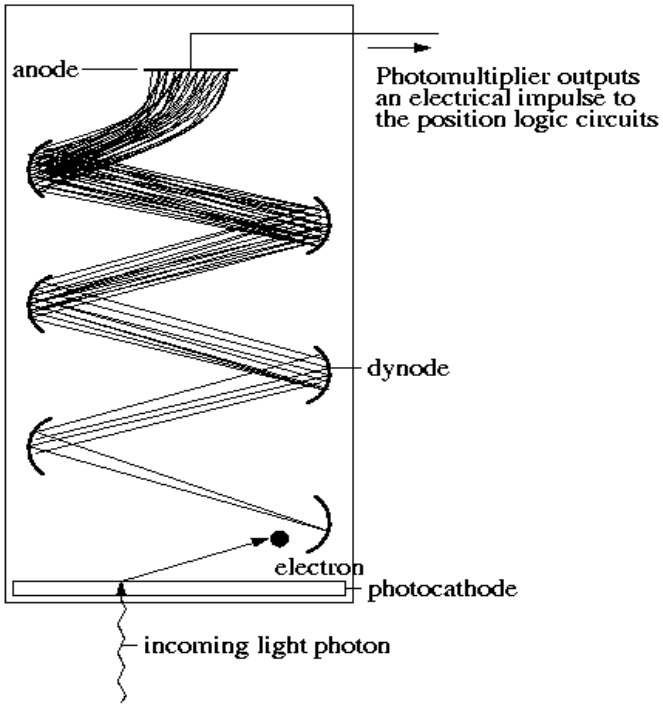

A Photomultiplier Tube

Fig. 2: A Photomultiplier Tube

Each gamma camera has several photomultiplier tubes arranged in a geometrical array. The typical camera has 37 to 91 PMT's (*see Fig. 3 bellow*).

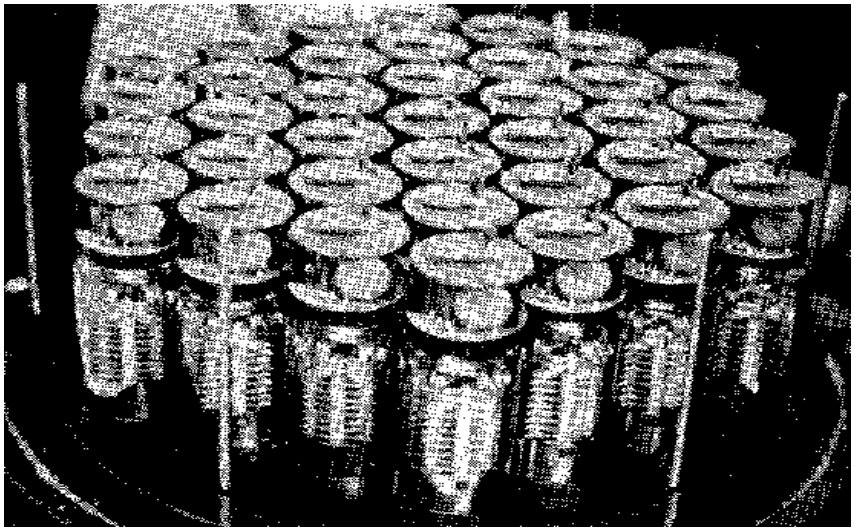

Fig. 3: A Photomultiplier Tube Array

4. Position Circuitry

The position logic circuits immediately follow the photomultiplier tube array and they receive the electrical impulses from the tubes in the summing matrix circuit (SMC). This allows the position circuits to determine where each scintillation event occurred in the detector crystal.

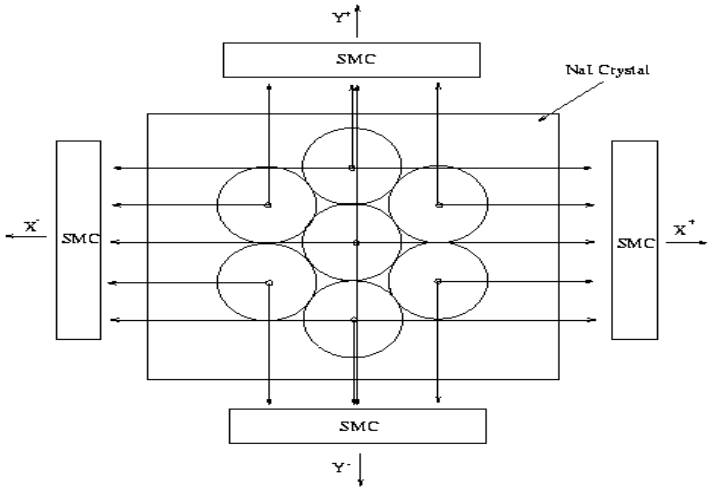

Fig. 4: Position circuits

5. Data Analysis Computer

Finally, in order to deal with the incoming projection data and to process it into a readable image of the 3D spatial distribution of activity within the patient, a processing computer is used. The computer may use various different methods to reconstruct an image, such as filtered back projection or iterative reconstruction, both of which are further described in this thesis.

Acquisition Protocols

Various different acquisitions can be performed with a SPECT camera.

1. Planar Imaging

The simplest acquisition protocol is the ***planar*** image. With planar imaging, the detector array is stationary over the patient, and acquires data only from this one angle. The image created with this type of acquisition is similar to an X-ray radiograph. Bone scans are done primarily in this fashion.

2. Planar Dynamic Imaging

Since the camera remains at a fixed position in a planar study, it is possible to observe the motion of a radiotracer through the body by acquiring a series of planar images of the patient over time. Each image is a result of summing data over a short time interval, typically 1-10 seconds. If many projections are taken over a long time, then an animation of the tracer movement can be

viewed and data analysis can be performed. The most common dynamic planar scan is to measure ***glomerular filtration rate*** in the kidneys.

3. SPECT Imaging

If one rotates the camera around the patient, the camera will acquire views of the tracer distribution at a variety of angles. After all these angles have been observed, it is possible to reconstruct a three dimensional view of the radiotracer distribution within the body. This will be further explained in reconstruction of images.

4. Gated SPECT Imaging

As the heart is a moving object, by performing a regular SPECT of the heart, the end image obtained will represent the average position of the heart over the time the scan was taken. It is possible to view the heart at various stages of its contraction cycle however, by subdividing each SPECT projection view into a series of sub-views, each depicting the heart at a different stage of it's cycle. In order to do this, the SPECT camera must be connected to an ECG machine which is measuring the heart beat. In non-gated SPECT imaging one projection image is acquired at each angular step along the acquisition orbit. With gated SPECT, data acquired during each angular step is further subdivided into a specific phase of the cardiac cycle (typically 8 or 16 phases) based upon the R-R interval. 16 phase data sets are required for diastolic function assessment, but

can suffer from low counts. Summing the data from the individual phases will produce a standard SPECT image, but ventricular function data can also be assessed by review of the gated data set. Gated imaging data can add important independent and incremental prognostic information to the data obtained from the perfusion examination. Irregular arrhythmias such as atrial fibrillation and ventricular ectopy produce "flickering" in the rotating summed projection cine images. This is due to the back-projection of varying data indicating count inconsistencies have occurred at different projection images. On the other hand, regular arrhythmias such as a tachy/brady arrhythmia are not associated with "flickering" and may be overlooked. For patients with severe arrhythmias (particularly atrial fibrillation) it is recommended that myocardial perfusion SPECT imaging NOT be performed with ECG gating due to an apparent worsening of the perfusion pattern on summed gated images.

Reconstruction

The most common algorithm used in the tomographic reconstruction of clinical data is the filtered backprojection method. In recent years the iterative reconstruction methods are also used. The most widely used acceleration technique is the ordered subset procedure of Hudson and Larkin, which resulted in the development of the ordered-subset expectation maximization (OSEM) technique. The OSEM algorithm recently has become available on

many commercial nuclear medicine computer systems and is now being used in routine clinical practice. Further discussion of the two reconstruction methods compared in this study is found in chapter 2.

SPECT Applications

These are some examples of the studies that can be performed with a SPECT camera.

1. Heart Imaging

Figure 5 is Tc-99m-myocardial MIBI scan taken under stress conditions. Regions of the heart that are not being perfused display as cooler regions.

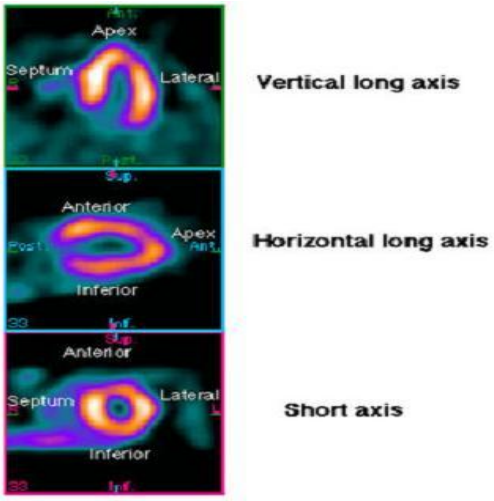

Fig. 5: MIBI scan

2. Brain Imaging

Figure 6 is a Tc-99m- HMPAO transverse SPECT image of the brain. Note the hot spots present in the right posterior region.

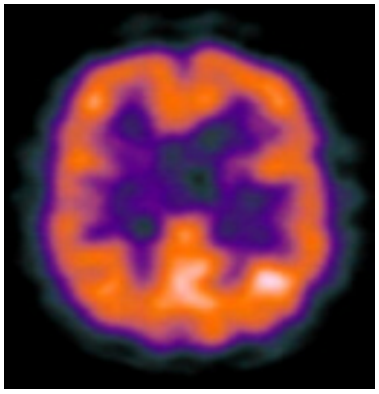

Fig. 6: Transverse SPECT image of the Brain.

3. Kidney/Renal Imaging

Figure 7 is a renal planar scan using Tc-99m MAG3 tracer (a glucose analogy).

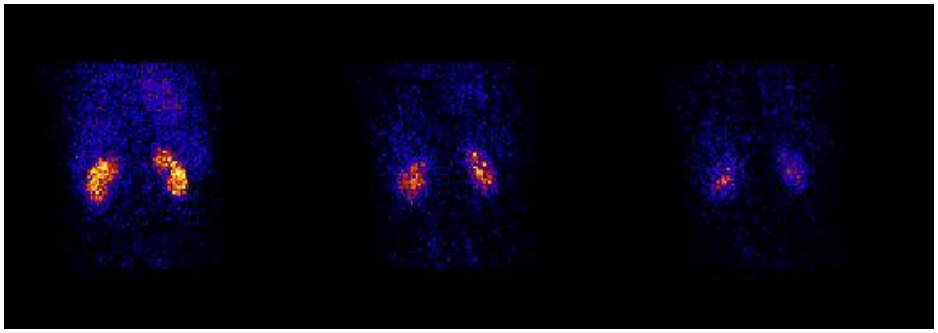

Fig. 7: Renal scan

4. Bone Scans

Bone scans are typically performed in order to assess bone growth and to look for bone tumours. The tumours are the dark areas seen in figure 8 below.

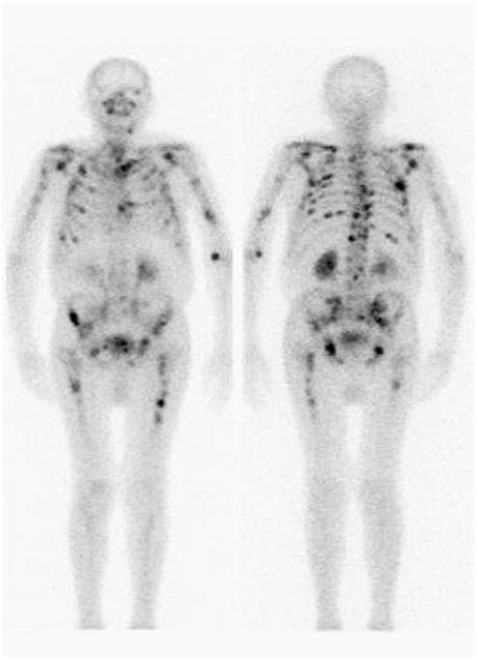

Figure 8: Bone scan

In this study, the emphasis is on comparison between FBP and OSEM in reducing bladder artifact in pelvic SPECT imaging.

Pelvic imaging using SPECT is plagued by the presence of the "bladder-filling" artifact. Bone imaging of the pelvis is an important diagnostic test for the detection of avascular necrosis of the femoral heads and for the detection of metastatic tumours and other diseases such as osteomyelitis. Planar imaging is possible, but SPECT offers improved sensitivity and specificity because it has greater contrast and allows differentiation of overlying internal structures. When SPECT has been available, its sensitivity in the detection of avascular necrosis has been shown to be 85%, compared with 55% for planar imaging, with no loss of specificity [(1).] Two major obstacles limit SPECT of the pelvis: the

inhomogeneous attenuation caused by the hip bones and pelvic girdle and the accumulation of activity in the bladder due to normal excretion of bone radiotracer throughout scanning. Both factors lead to inconsistencies in the projection data, which cause artifacts in the reconstructed image. These artifacts can appear as anomalous blobs of apparent activity, which may be mistaken for tumours (false positives), or as dark shadows, which can hide true lesions (false negatives)[2,3] and mimic the photon-deficient regions of avascular necrosis [4]. The bladder-filling artifacts that occur in pelvic imaging are particularly severe, rendering as many as 20% of SPECT scans of this region unusable [1].

Attenuation correction (AC) has been shown to improve bone SPECT image quality in other regions of the body, such as the cervical spine [5,6], and to improve lesion detection in thoracic SPECT [3]. PET images of the pelvis have also been shown to benefit from AC [7]. Unfortunately, AC alone may not be sufficient for SPECT because changing activity in the bladder throughout the acquisition contributes to the artifact. Catheterization is a possible means of mediating the effect caused by accumulation of activity in bladder due to normal excretion of bone radiotracer throughout scanning, but it has an associated increased risk of complications such as infection and consequently is unattractive for general application. Different techniques of digital filtering

have been suggested to correct for this artifact [4, 8] but have had limited success [9]. These approaches try to correct for the artifact after image creation and do not address the issue of the changing bladder-activity levels[47]. A different approach is that of Penney et al. [10], who attempted to reduce the inconsistencies in the data by acquiring multiple fast-rotation images, that is, a dynamic SPECT acquisition. By acquiring 10 complete SPECT scans over the course of 30 min; Penney et al. were able to reduce the artifact by 50%. Faster scans, with even less change in bladder activity from start to finish, should further reduce the impact of the artifact. Unfortunately, fast-rotation continuous imaging, a technique for performing dynamic SPECT, requires specialized hardware and is consequently not available in most nuclear medicine departments.

For almost 20 years, filtered back projection (FBP) has been the standard technique for tomographic image reconstruction in clinical nuclear medicine. However, FBP can result in the generation of artifacts, which mainly consist of streaking and negative counts near the borders of hot objects [11, 12]. There are myriad iterative reconstruction algorithms that can be used as alternative reconstruction techniques to FBP. However, many of these, such as maximum likelihood expectation maximization (MLEM), are computationally intensive and have never been used in clinical practice [13]. Various methods have been

developed to accelerate the speed of these algorithms. The most widely used acceleration technique is the ordered subset procedure of Hudson and Larkin [14], which resulted in the development of the ordered-subset expectation maximization (OSEM) technique. The OSEM algorithm recently has become available on many commercial nuclear medicine computer systems and is now being used in routine clinical practice [15, 16].

An OSEM technique has been used increasingly in reconstruction of bone and myocardial perfusion SPECT images and has been shown to be more accurate than FBP even in cases of incomplete datasets. OSEM may help to address this poor record of bladder artifacts, which render up to 20% of the images unreadable. Iterative reconstruction may be the most effective method at removing bladder artifacts in clinical pelvic SPECT and thus implemented in routine bone SPECT processing.

In this study, using multiple data replicates, we will investigate the performances of OSEM reconstruction schemes in pelvic SPECT. We will compare the performance of various combinations of OSEM number of iterations and subsets, with performance obtained with FBP. The choice of the number of (subset x iteration) to be used for OSEM reconstruction will be guided by the its correlation with the Acetabulum/Bladder ratio. The motivation for conducting this study is to answer two practical questions

"Is OSEM reconstruction truly a viable alternative to FBP reconstruction in qualitative and semi-quantitative pelvic SPECT imaging studies in the case of bladder artifacts?"

"What is the optimal number of iterations and subsets to be chosen for reconstruction of pelvic SPECT images?"

CHAPTER 2

LITERATURE REVIEW

A variety of imaging systems rely on reconstruction of an image from its projections through the process of computed tomography (CT). In medical imaging, for example, X-ray CT scans, magnetic resonance imaging (MRI), and various types of positron emission tomography (PET) all record two-dimensional projections of a three dimensional object. No single projection uniquely defines the object being imaged. In fact, in the absence of any assumptions about the object being imaged, no finite number of projections defines the original object uniquely and exactly. By combining information from a number of projections, however, one can produce an accurate description of the object being imaged. A similar problem occurs in astronomy, where one might combine images of a heavenly body taken at different times from slightly different angles, in order to obtain a composite image far more accurate than the originals. In radar imaging, one may again wish to combine a number of images obtained at different angles. While these scenarios differ substantially from one another, they present similar mathematical problems which can be solved using similar techniques.

Most medical imaging systems separately reconstruct two-dimensional slices of a three-dimensional object. If necessary, these reconstructed two-dimensional slices may be combined to create a three-dimensional representation of the object being imaged. Medical CT systems rely on two basic imaging modalities: transmission tomography and emission tomography[10]. In transmission tomography, beams of radiation, such as X-rays, are passed through the body being imaged from various positions and at various angles. Each beam is detected on the side of the body opposite from the beam source, and its detected intensity is compared to its intensity at the source. If g, the transmittance of the object, is defined as the logarithm of the ratio of the intensity of the detected beam to the intensity of the emitted beam, then g is given by the linear transformation

$$g = \int_L f(x, y)\, du, \qquad (1)$$

where $f(x,y)$ is the absorption coefficient of the object at the point (x,y) and L is the line along which the beam travels. Imaging systems such as CT scanners obtain g for various lines L, and use this information to compute an approximation to $f(x,y)$ throughout the object.

Emission tomography, on the other hand, measures radiation emitted by an object of interest in various directions. In medical tomography, for example, a patient may be injected with a radioactive substance which enters the

bloodstream. A movable array of detectors measures radiation arriving at each point from a direction perpendicular to the detector array (Fig. 9). Thus, at any given position of the detector array as it is rotated around the object, each detector measures radiation emitted by sources along a straight line. In the absence of attenuation, and with ideal detectors, the detected intensity will sum linearly along this line. If we denote this intensity g, then again:

$$g = \int_L f(x, y)\, du, \qquad (1)$$

where $f(x,y)$ represents the concentration of the radioactive substance at (x,y) and L represents the line passing through the detector perpendicular to the detector array.

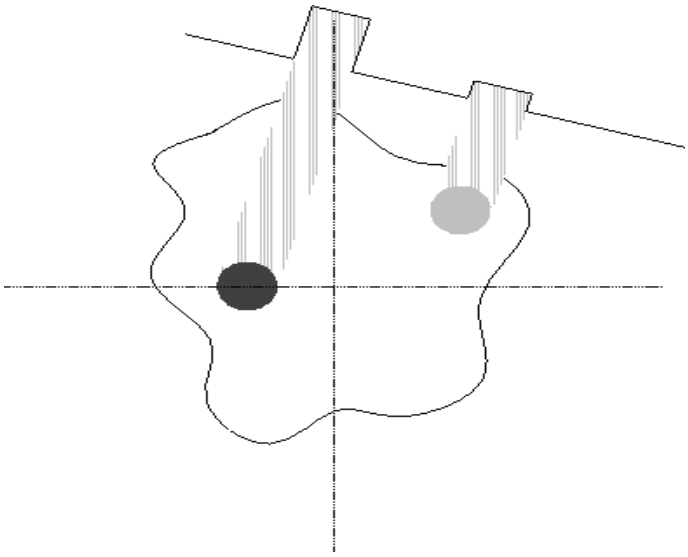

Fig. 9: Detection of a projection in emission tomography.

In each case, the mathematical formula for projection is the same. In the two-dimensional case, the line *L* can be represented uniquely by the parameters *r* and θ, where θmeasures the counter clockwise angle of the line from the vertical, and *r* measures the distance of the line from the origin of the (*x*,*y*) plane. Thus, we can use the above formula to define a transform which maps a function *f*(*x*,*y*) to a function $g(r,\theta)$, where $g(r,\theta)$ is the line integral of *f*(*x*,*y*) over the line defined by *r* and θ. This transform is known as the Radon transform and denoted $\mathcal{R}$. (Fig. 10). It corresponds closely to an ``ideal'' parallel-beam imaging system, since in such a system, each projection of the image corresponds to a slice through the radon transform at constant θ. The basic, idealized problem of tomography is to reconstruct an image from its Radon transform. Fortunately, the Radon transform, when properly defined, has a well-defined inverse [17]. In order to invert the transform, one needs projection data spanning 180 degrees.

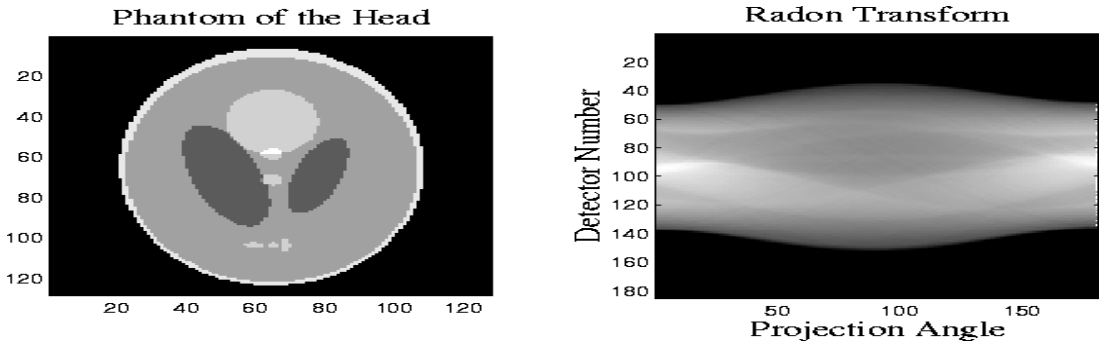

Fig. 10: The Shepp-Logan head phantom and its radon transform. $\theta$is the counterclockwise angle from the horizontal to the line on which the detector array is located.

Unfortunately, the actual data detected by a medical imaging system does not correspond exactly to the Radon transform of the ``true'' image. In any imaging system, projection data will be corrupted by noise, and the projections are measured with only limited resolution. The geometry of the imaging system may differ from the ideal, particularly in transmission tomography, where a fan beam imaging system is more easily implemented than a parallel-beam system. Emission tomography suffers from the problem of attenuation. Since the object being imaged will itself absorb some of the emitted radiation, the observed intensity of a radioactive source depends on its distance from the detector and on the density of the substance between the detector and the source. In any type of tomography, the projection angles available may be limited. One may need to reconstruct an image from only a few projections, or from projections spanning only a small range of angles. In astronomical imaging, for example, one cannot necessarily obtain images of a heavenly body from all angles. Thus, the suitability of a reconstruction technique must be judged not only by its performance in the ideal case, but also by its potential to adapt to real imaging systems which differ from the ideal.

In developing reconstruction techniques, we worked with real data from a SPECT system. The SPECT medical imaging system detects gamma rays emitted by a radioactive source. The camera head rotates around the subject. At each

projection angle, gamma rays entering the camera head pass through an array of collimators which transmit only photons travelling in a direction perpendicular to the projection plane. The transmitted gamma rays then strike an array of fluorescent crystals. Photomultiplier tubes detect photons emitted by the crystals, localizing the location at which the original gamma ray struck the crystal sheet. Thus, this system produces projections with a parallel-beam geometry. From these projections, one can compute the distribution of radioactive emitters in the original image.

Single photon emission computed tomography (SPECT, or less commonly, SPET) is a nuclear medicine tomographic imaging technique using gamma rays. It is very similar to conventional nuclear medicine planar imaging using a gamma camera. However, it is able to provide true 3D information. This information is typically presented as cross-sectional slices through the patient, but can be freely reformatted or manipulated as required.

SPECT is superior to planar imaging with regard to disease localization. It improves object contrast (i.e. contrast resolution or the target to background ratio) by removing overlying tissues.

Images of the inside of the human body can be obtained noninvasively using tomographic acquisition and processing techniques. In particular, these

techniques are commonly used to obtain images of a γ-emitter distribution after its administration in the human body. The reconstructed images are obtained given a set of their projections, acquired using rotating gamma cameras. A general overview of analytic and iterative methods of reconstruction in SPECT is presented with a special focus on FBP and OSEM. The FBP algorithm is faster than iterative algorithms, with the latter providing a framework for accurately modelling the emission and detection processes.

In pelvic bone SPECT using Tc-99m labelled compounds, the dynamic accumulation of activity into the bladder during the data acquisition process often results in data inconsistencies in the projections and consequently artifacts which may be significant enough to impair lesion detection. Comparison of FBP and OSEM reconstructions in reducing bladder artifacts in pelvic bone Tc-99m SPECT is essential for the evaluation of the image quality in either of the reconstruction method used. This in turn will enable proper interpretation of the images subsequently proper management of patients.

Filtered back-projection:

It involves:

1. Data Projection

As a SPECT camera rotates around a patient, it creates a series of planar images called projections. At each stop, only photons moving perpendicular

to the camera face pass through the collimator. As many of these photons originate from various depths in the patient, the result is an overlapping of all tracer emitting organs along the specific path, much in the same manner that an X-ray radiograph is a superposition of all anatomical structures from three dimensions into two dimensions. A SPECT study consists of many planar images acquired at various angles. The figure below displays a set of projections taken of a patient's bone scan.

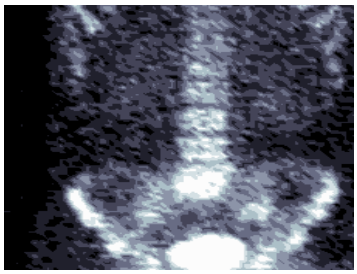

Fig. 11: Single Projection of the Bone scan

After all the projections are acquired, they are subdivided by taking all the projections for a single, thin slice of the patient at a time. All the projections for each slice are then ordered into an image called a sinogram as shown in figure 12. It represents the projection of the tracer distribution in the body into a single slice on the camera at every angle of the acquisition.

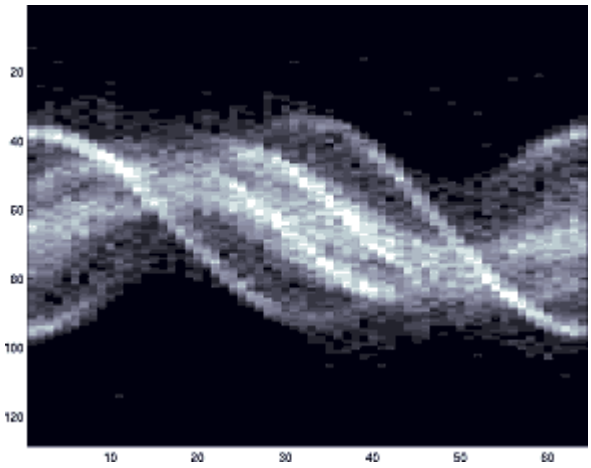

Fig. 12: Sinogram

The aim of the reconstruction process is to retrieve the radiotracer spacial distribution from the projection data.

2. Fourier Transform of Data

If the projection sinogram data were reconstructed at this point, artifacts would appear in the reconstructed images due to the nature of the subsequent backprojection operation. Additionally, due to the random nature of radioactivity, there is an inherent noise in the data that tends to make the reconstructed images rough. In order to account for both of these effects, it is necessary to filter the data. When we filter data, we can filter it directly in the projection space, which means that we convolute the data by some sort of smoothing kernel.

Convolution is a computationally intensive task however and so it is useful to avoid using it when possible. It turns out that the process of convolution in the

spatial domain is equivalent to a multiplication in the frequency domain. This means that any filtering done by the convolution operation in the normal spatial domain can be performed by a simple multiplication when transformed into the frequency domain.

In SPECT imaging we make a transform of the projection data into the frequency space whereby we can more efficiently filter the data. The transform that we make use of is called the one dimensional Fourier Transform.

3. Data Filtering

Once the data has been transformed to the frequency domain, it is then filtered in order to smooth out the statistical noise. There are many different filters available to filter the data and they all have slightly different characteristics. For instance, some will smooth very heavily so that there are not any sharp edges, and hence will degrade the final image resolution. Other filters will maintain a high resolution while only smoothing slightly. Some typical filters used are the Hanning filter, Butterworth filter, low pass cosine filter, Weiner filter, etc. Regardless of the filter used, the end result is to display a final image that is relatively free from noise and is pleasing to the eye.

4. Inverse Transform of the Data

As the newly smoothed data is now in the frequency domain, it must be transformed back into the spatial domain in order to get out the x,y,z information regarding spatial distribution. This is done in the same type of manner as the original transformation is done, except using what is called the one dimensional inverse Fourier Transform. Data at this point is similar to the original sinogram except it is smoothed.

5. Backprojection

The main reconstruction step involves a process known as backprojection. As the original data was collected by only allowing photons emitted perpendicular to the camera face to enter the camera, backprojection smears the camera bin data from the filtered sinogram back along the same lines from where the photon was emitted from. Regions where backprojection lines from different angles intersect represent areas which contain a higher concentration of radiopharmaceutical.

Mathematically, filtered backprojection as a concept is relatively easy to understand. Assuming that there is finite number of projections of an object which contains radioactive sources (Fig. 13 A). The projections of these sources at 45 degree intervals are represented on the sides of an octagon. Figure 13 B illustrates the basic idea behind back projection, which is to simply run the

projections back through the image (hence the name ``back projection'') to obtain a rough approximation to the original. The projections will interact constructively in regions that correspond to the emittive sources in the original image. A problem that is immediately apparent is the blurring (star-like artifacts) that occur in other parts of the reconstructed image. One would expect that a high-pass filter could be used to eliminate blurring, and that is the case. The optimal way to eliminate these patterns in the noiseless case is through a ramp filter [18]. The combination of back projection and ramp filtering is known as filtered back projection.

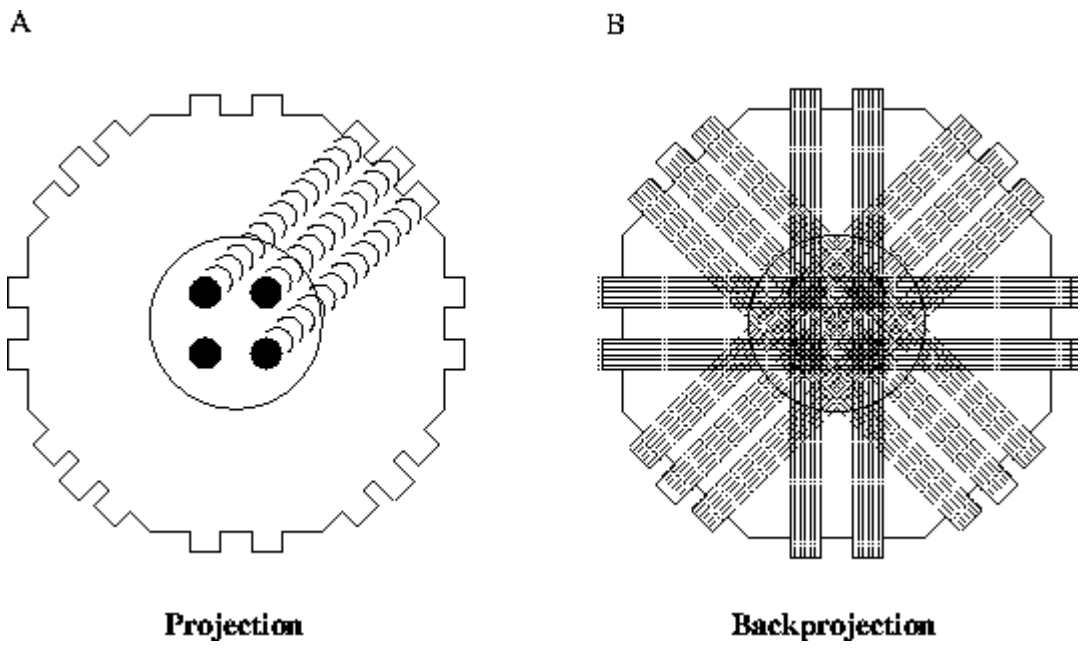

Fig. 13: Illustration of back projection

For parallel beam tomography the projections can be expressed as the Radon transform of the object that is to be reconstructed. The Radon transform is defined as:

$$g(s,\theta) = \mathcal{R}(f) = \int_{-\infty}^{\infty}\int_{-\infty}^{\infty} f(x,y)\delta(x\cos\theta + y\sin\theta - s)\,dxdy, \qquad (2)$$

i.e., the line integral along a line (a tomography beam) at an angle θ from the y-axis and at a distance $|s|$ from the origin. By rotating the coordinate system,

$$\begin{aligned} s &= x\cos\theta + y\sin\theta \\ u &= -x\sin\theta + y\cos\theta \end{aligned}$$

or

$$\begin{aligned} x &= s\cos\theta - u\sin\theta \\ y &= s\sin\theta + u\cos\theta \end{aligned}$$

then

$g(s,\theta)$

can be expressed as

$$g(s,\theta) = \int_{-\infty}^{\infty} f(s\cos\theta - u\sin\theta, s\sin\theta + u\cos\theta)\,du \qquad (3)$$

One of the approaches for reconstructing the image is to take the inverse Radon transform of the projections. This involves two steps; the image is back projected and then filtered with a two dimensional ramp filter.

The back projection operator, $\mathcal{B}$is defined as

$$\mathcal{B}g = \int_0^{\pi} g(x\cos\theta + y\sin\theta)\,d\theta. \qquad (4)$$

This operator represents the accumulation of the projections that pass through the point (x,y). As in the example above, the back projection is a blurred version of the desired image.

$$\hat{f}(x,y) = \mathcal{B}g = \mathcal{B}\mathcal{R}f = f(x,y) * *(x^2+y^2)^{-\frac{1}{2}} \qquad (5)$$

The image can be now unblurred with a two-dimensional ramp filter. Because two-dimensional filtering is computationally intensive, a better a better approach is to reverse the order of the filtering and the back projection. The second approach is possible due to the projection slice theorem, which states that the one-dimensional Fourier transform with respect to s of $g(s,\theta)$ is equal to the central slice at angle θ of the two-dimensional Fourier transform of f(x,y),

$$\mathcal{F}[g(s,\theta)] = \mathcal{F}_2[f_x cos\theta, f y sin\theta]. \qquad (6)$$

The projection slice theorem implies that the Radon transform of the two-dimensional convolution of two functions is equal to the one-dimensional convolution of their Radon transforms. Convolution has the nice property of being symmetric, i.e $f*g=g*f$. This can be used to find a closed formula for the inverse Radon transform. It also implies a simpler inverse Radon scheme than before. It can be summarized with the following two points:

1. Do a one-dimensional high-pass filtering of each projection using a ramp filter.
2. Back project the outputs of the filter.

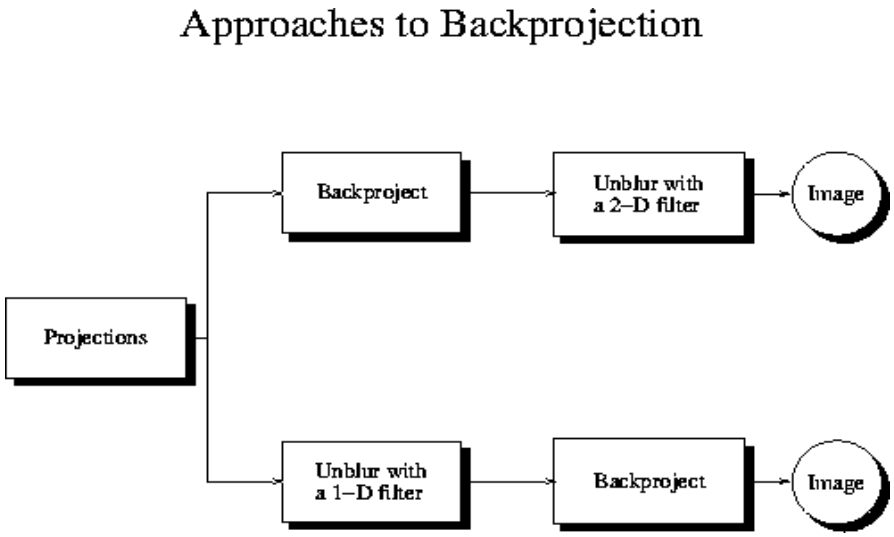

Figure 14: Illustration of the two possible cases for filtered back projection. Most algorithms today does a one-dimensional filtering of the projections before the back projection.

In implementing the back projection algorithm, the following has to be considered:

Interpolation: The sum over all pixels, of all the rays that passes through a particular pixel, has one minor problem: $g(s,\theta)$ and f(x,y) are in different coordinate systems. It will, however, require interpolation of $g(s,\theta)$ to points between the actual data points. The best type of interpolation is linear interpolation.

Centering: Proper correction for centering is crucial to the success of the back projection algorithm. Even a small error causes severe artifacts.

Matrix formulation: A straightforward implementation of the back projection operation uses three nested loops, looping over each pixel in the image, and for each pixel, through the different angles of θ.

Filtering: As mentioned previously, the back projection operation produces a blurred version of the desired image. In the absence of noise, the desired image can be obtained by filtering the back projection with a ramp filter. Unfortunately, the high-pass nature of the ramp filter leads to amplification of high-frequency noise.

All real data will be corrupted in some way by attenuation. There are several algorithms that compensate for this. These are usually post-processing techniques that operate on the output of the filtered back projection. A very widely used method is Chang's method, [19]. This method assumes constant attenuation throughout the whole object. Each pixel within the object of interest is simply multiplied by a correction coefficient. These coefficients can be expressed as:

$$C(x,y) = [\frac{1}{M} \sum_{i=0}^{M} e^{-\mu l(x;y;\theta i)}]^{-1} \qquad (8)$$

where $l(x,y,\theta)$ is the distance that the projection *i* goes through the attenuating material, M is the total number of projections, and u is an attenuation factor, typically assumed to be .11 cm^{-1}. C(x,y) will be based on

the average of the attenuation of all the projections that passes through the point.

Summary in FBP

Filtered back-projection is used for image reconstruction. As explained above Back-projection alone (without filtering) results in undesirable image smoothing and the presence of star-like artifacts. The degree to which back-projection artifacts can be removed must be balanced by the degree to which image noise can be tolerated. Frequency refers to the change in number of counts from pixel to pixel. True image signal falls off rapidly with increasing frequency, while the noise content remains constant. Background (noise) is considered to be high frequency because there is marked variability in the number of counts from pixel to pixel. Image sharpness (edge detection, small objects, and fine detail) are also high frequency, while the target (a large object) is low frequency. RAMP filters (high pass filters) boost high frequencies in order to sharpen the spatial details (edges) of the image and to minimize the star artifact. Unfortunately, this also increases the noise because the filter linearly enhances higher frequencies. To limit this effect (i.e. to decrease the noise) a second roll-off or low pass (or "smoothing") filter is applied. Low pass filters are typically applied to projection images **before** reconstruction to reduce noise early in the processing chain. Common low pass filters include:

Butterworth, Hanning, Shepp-Logan, and Parzen. Butterworth filters are the most commonly used for nuclear medicine procedures.

Filtering prior to back projection is preferable because:

1- It reduces the propagation of noise at an earlier stage in the image formation process and
2- It promotes the implementation of a filter symmetric in 3-dimensions.

Iterative reconstruction:

These are algebraic reconstruction techniques, which use projection images as input, but aim at finding the exact mathematical solution to the problem of activity distribution in the field of view by considering the value in each pixel of the reconstructed image as an unknown and each point in a profile as an equation. In brief, the value of all pixels is initially guessed using filtered back projection; then those initial values are slightly altered several times (iterations) until they converge to a final result consistent with the available count profiles. Iterative reconstruction is intrinsically slower than filtered back projection, but it has the clear advantage of reducing reconstruction artifacts-

such as those caused by hepatic or extra cardiac activity on myocardial perfusion, and bladder artifacts in pelvic bone imaging.

A major advantage with algebraic reconstruction methods over the filtered back-projection method is that algebraic methods can be adapted easily to account for non-ideal responses of the imaging system. As an example, consider the problem of attenuation in emission tomography, assuming that the attenuation profile of the object being imaged is known. The reconstruction problem can be formulated in the same fashion as described in the previous section, but the pixel weights assigned by the projection operator R_i will now depend on the distance between the pixel and the detector, and the assumed attenuation profile. Unlike Chang's method, which involves averaging correction factors, this method allows an exact attenuation correction. The matrix *W* used for the reconstructions in this project has been corrected for attenuation using the same assumptions (uniform attenuation within the phantom) as in the case of the filtered back projection method, allowing a direct comparison of the results. If a real attenuation profile were known, however, it could be corrected for in the same way. Interestingly, some of the most advanced gamma cameras available today provide this information by performing simultaneous SPECT and transmission scans using multiple energy windows.

The formation of the matrix *W* and the calculation of the appropriate weights was found to be one of the more time consuming parts of this algorithm, since it required loops nested in several levels. This was therefore implemented in C in order to reduce computation time.

The ability of the algebraic method to correct for imperfections in the imaging system are not limited to attenuation. If the response of the imaging system deviates from the ideal Radon transform for other reasons, such as the geometric arrangement of the detectors, the general matrix formulation still applies. This is in contrast to the filtered back-projection method which is based on the inverse Radon transform.

Iterative reconstruction algorithms for nuclear medicine are finding wider use in both research and commercial products, as procedures for nonuniform attenuation compensation become more common place. The lineage of the most widely used iterative reconstruction algorithms can be traced back to the maximum-likelihood expectation maximization (MLEM) algorithm. Ordered-subset algorithms, which are related to but much faster than MLEM, have quickly become the dominant iterative reconstruction procedures in both PET and SPECT in recent years. These algorithms include the ordered-subset EM (OSEM) algorithm and the rescaled block-iterative EM (RBIEM) algorithm. The OSEM algorithm has been chosen both for its impressive speed, usually

requiring fewer than 5 iterations to reach a usable solution, and for its relative simplicity of implementation.

The choice of which parameters to employ in OSEM algorithm during image reconstructions is not entirely obvious. The problem is intrinsically multifactoral: OSEM results depend not only on subset and number of iterations but also on pixel size and amount of post reconstruction filtering as well as the amount of counts acquired per pixel. According to OSEM theory, in noiseless circumstances the effect of subset and number of iteration should be additive over noise. In the present work OSEM performances are characterized with respect to subset and number of iterations, having fixed the pixel size and the amount of post reconstruction filtering.

Tomographic Reconstruction:

Reconstructed images typically have image matrixes of 64x64 or 128x128 pixels, with the pixel sizes ranging from 3-6 mm. The number of projections acquired is chosen to be approximately equal to the width of the resulting images. In general, the resulting reconstructed images will be of lower resolution, have increased noise than planar images, and be susceptible to artifacts.

Scanning is time consuming, and it is essential that there is no patient movement during the scan time. Movement can cause significant degradation

of the reconstructed images, although movement compensation reconstruction techniques can help with this. A highly uneven distribution of radiopharmaceutical also has the potential to cause artifacts. A very intense area of activity (e.g. the bladder) can cause extensive streaking of the images and obscure neighbouring areas of activity. This is a limitation of the FBP reconstruction algorithm. Iterative reconstruction (in this case OSEM) is an alternative algorithm which is growing in importance, as it is less sensitive to artifacts and can also correct for attenuation and depth dependent blurring. Attenuation consists of photon absorption as well as Compton scatter. Compton scatter not corrected for may result in inappropriate attenuation corrections being applied. Scattered photons originating from the bladder can also result in artefacts being created in the skeletal areas.

The uniformity requirements for SPECT with FBP are highly dependent on the noise characteristics of the reconstructed data [20, 21]. There are significant differences in the noise characteristics of FBP and OSEM algorithms, particularly at low counting rates [22]. While non uniformities in the planar data would be expected to result in artifacts in the data reconstructed using OSEM, the magnitude and nature of these artifacts is not well known. Although the uniformity requirements of the FBP technique have been well studied [23,24], at present it is unclear how the uniformity requirements associated with the

OSEM technique are, compared with those associated with the FBP technique. The aim of this study is to compare lesion detectability on images reconstructed with OSEM over those reconstructed with algorithm based on FBP and to optimize pelvic SPECT by reducing bladder artefacts using various OSEM reconstruction parameters.

Pelvic bone SPECT using Tc-99m labelled compounds is a non-trivial imaging procedure due to two confounding issues.

Firstly, the attenuation of emitted activity due to non-homogenous attenuation distribution may result in inconsistent projection measurements of the radiotracer distribution. As a result of these inconsistent measurements, it is possible for streaking artifacts to appear in reconstructed images, which may reduce lesion contrast within the pelvic region [25]. This effect may be reduced by acquiring transmission measurements using an external radioactive source, and incorporating attenuation compensation into the image reconstruction process.

Another issue in pelvic SPECT however, is in inconsistent projection data being acquired as a result of accumulation of activity into the bladder during the data acquisition process. When reconstructed with conventional image reconstruction procedures such as FBP, again, image artifacts will appear as streaks through the bladder region [26]. The extent of these streaks is

dependent upon both the amount of activity accumulating in the bladder as well as on the rate of uptake of activity into the bladder. When either the amount or rate of uptake is not significant, these streaks will not appear significant. In many cases however, the amount and/or rate of uptake is significant and produce streak artifacts. These artifacts may mask other regions within the pelvis, thus possibly reducing lesion detection.

The performances of OSEM and FBP have been compared in a number of other experimental and clinical studies, [27 - 31] with a variety of reconstruction parameters employed with OSEM, including number of subset, number of iteration and the type and amount of post reconstruction smoothing to replace noise with increasing number of iterations. But no consensuses have been reached.

Blocklet et al. [32] compared FBP and OSEM (8 subsets and 2 iterations without post filtering) in bone SPECT reconstruction; Case et al.[33] compared attenuation correction techniques in bone SPECT of the spine using OSEM (12 subsets and 3 iterations, 3D Wiener filter); Kauppinen et al. [34] compared FBP and OSEM (6 subsets and 4–12 iterations, Butterworth post filtering) in brain perfusion SPECT with scatter and non uniform attenuation correction; Vanhove et al.[35] implemented OSEM algorithm for data acquired with a pinhole collimator in phantom studies: using OSEM different iterations were used in

combination with 1–32 subsets. Wells et al. [36] compared FBP and OSEM (8 subsets and 1 iteration, 3D Gauss) for small-lesion detection and localization in 67Ga SPECT.

Van Der Weerdt et al [37] had an opinion that the choice of applied OSEM parameters is a good compromise reaching sufficient (but not full) convergence and restricting noise within acceptable levels for the purpose of clinical evaluation. They went further stating that, the use of OSEM reconstruction for quantitative (dynamic) studies without ensuring full convergence and fully validating the effects of OSEM reconstruction parameters on the accuracy and precision of these types of scans is strongly discouraged. [38, 39, 40]

To date reconstruction of pelvic SPECT studies is performed primarily using FBP. This method is fast, robust, linear and yields reliable quantitative results. However, for data with poor statistics, such as intense bladder uptake data, FBP results in poor image quality because of streak artifacts and low signal-to-noise ratio (SNR). Maximum likelihood expectation maximization (MLEM) iterative reconstruction for emission tomography was first developed by Shepp and Vardi [41]. Hudson and Larkin [42] proposed an OSEM implementation of the algorithm. Introduction of the latter algorithm decreased the reconstruction time considerably and made it feasible to apply OSEM in daily clinical routine.

Many comparison studies showed that iterative reconstruction outperforms FBP in terms of image quality, signal-to-noise ratio, resolution and contrast [43] and improves lesion detection. [44] They highlighted that the characteristics of the reconstructed images are bound to the chosen number of iterations and to the source distribution [45]. The convergence studies showed that the optimal number of iterations depends on the statistics of the input scan. The better count statistics, the higher the number of iterations is to be used [46].In the previous studies, determining the number of iterations and subsets enabling the most accurate parameter estimation was never validated [46]. The optimal number of MLEM equivalent updates (iterations x subsets) is object dependent and convergence does not occur at the same iteration for the whole image. The finding of the most appropriate parameters is even more complicated for bladder artifacts.

Accurate and reliable lesion detectability on images is important to guide therapeutic management, improve risk stratification, and provide prognostic information in the pelvic evaluation of patients. Hence it is crucial that the results are reliable and reproducible.

In this study, using clinically acquired pelvic bone SPECT data a hundred and five patient datasets were compared using two reconstruction methods: the

filtered backprojection (FBP) and ordered subset expectation maximization (OSEM).

CHAPTER 3

MATERIALS AND METHODS

AIM

To evaluate the relationship of the bladder to acetabulum ratio in guiding the choice of the number of iterations and subsets used for OSEM reconstruction, for reducing bladder artifacts found on FBP reconstruction.

PATIENT SELECTION

105 patient 56% females and 44% males were recruited in the study prospectively between October 2008 and March 2009. The average age was 55years with a standard deviation of 15 years. Participant recruitment was from adult patients already scheduled for bone scanning in our department. All routine pelvic SPECTs and patients who, after plannar imaging, had pelvic lesions that could not be confidently identified due to bladder artifacts were included in the study. Each patient received 925MBq of Tc-99m-Methylene Diphosphonate (MDP) and was imaged 3 – 4 hours after injection. Our standard imaging procedure was followed, with each patient voiding his or her bladder immediately before imaging.

The Protocol and Informed consent of this study were considered by the Faculty of Health Sciences Research Ethics Committee, University of Pretoria and was found to be acceptable.

IMAGE ACQUISITION

Patients received 925MBq of Tc-99m-Methylene Diphosphonate (MDP) each, and plannar imaging was done 3 – 4 hours after injection. Planar imaging was done using one of the four gamma cameras; three of which are dual head (one GE Infinia Hawkeye ^{TM} and two E-Cam Siemens Medical Systems) and one single head all purpose camera (GE Millenium ^{TM}). Each was equipped with high – resolution, low energy collimators. A 256×1024 matrix with >1, 5 million counts was used when anterior or posterior whole body scanning was performed, in dual head cameras.

SPECT volumes are usually chosen following a visual assessment of the whole body planar scan. In this study the area of interest was the pelvic, so irrespective of the diagnosis of the patient, SPECT imaging was done to all patients found with equivocal planar lesions in the region of interest (the pelvis).

SPECT imaging was done on the E-Cam Siemens Medical System dual head cameras using a 128 x 128 matrix and a 6^0 step-and-shoot mode with counting

done at 30 seconds per step. Each head was set to rotate through 180^0 for a total of 360^0 SPECT acquisition, beginning from left and right lateral positions. The Butterworth filter was used for the images.

DATA/IMAGE ANALYSIS

Processing of SPECT images was done on the E- soft workstations by FBP and OSEM reconstruction methods. Images were analyzed in the same workstation using the 3DM SPECT program with attenuation correction. The planar images were used to determine the presence of equivocal lesions in the pelvis, which would need further assessment with SPECT imaging (see Fig. 15 to 18)

After the optimal reconstruction parameters have been determined for each imaging strategy, the methods were then compared using a human observer study in order to determine the best reconstruction strategy for the detection of lesions in the pelvic region.

The reconstructed images were evaluated subjectively with three nuclear medicine physicians, all of whom were familiar with these types of images. They were free to adjust windowing levels and choice of colour scale as desired. Blinded to the type of reconstruction used, they then labelled images from the best to the worst after which the data was analysed. Images were assessed on a 4-point scale for the presence of artifacts and the clinical impact

of artifacts on diagnosis of pelvic abnormalities. Clinical impact related to the location of the artifacts, for example, were artifacts present in a part of the image such that they would have influenced clinical evaluation of the image (e.g., evaluation for the presence of avascular necrosis)?

Clinical impact also referred to the impact of the artifact on the overall image quality; for example was there an increase in image noise distal to the artifact itself? On the 4- point scale, Grade 1 corresponded to Non-diagnostic image, Grade 2 to Poor quality image (Lesion/Background ratio <1), Grade 3 to Adequate quality image (Lesion/Background ratio = 1), and Grade 4 to Good quality image (Lesion/Background ratio >1).

The SPECT images were then reconstructed using 4 different iterations and subsets (2x8, 4x8, 3x12 and 6x12) which were chosen based on their correlation with the acetabulum/bladder ratio which was determined on the whole body images of each patient. These images were given to 3 Nuclear Physicians who were blinded to the study and they were asked to arrange the images from the best to the worst.

Reconstruction parameters are summarized in Table I.

Table I: Reconstruction Parameters

Method	Subset x Iteration
FBP	Not applicable
OSEM	2x8
	4x8
	3x12
	6x12

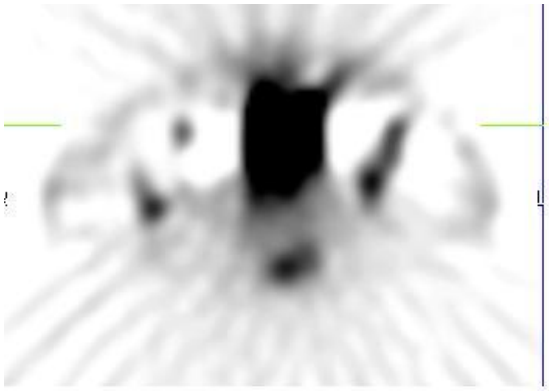

Fig. 15: Transaxial view of the pelvis reconstructed with FBP

Fig. 16: Transaxial view of the pelvis reconstructed with OSEM 8x2

Fig. 17: Trans axial view of the pelvis reconstructed with OSEM 8x4

Fig. 18: Transaxial view of the pelvis reconstructed with OSEM 12x3

CHAPTER 4

RESULTS

SPECT imaging was performed on a hundred and five patients. 59 of these patients were women and 46 were men (Table II) ranging in age between 17 years and 86 years old, mean age for the group was 55 years (Table III).

Table II: Gender Frequency

Demographics of study population		
Gender	59 female	46 male
Age	Avg 55 (+/-14.6)	Avg 55 (+/-17)

Table III: Summary for variables of Age (years) by categories of Gender

Gender	N	mean	Sd	min	max	p50
Female	59	55.72881	14.62736	22	86	55
Male	46	55.65217	17.71154	17	82	63
Total	**105**	**55.69524**	**15.9706**	**17**	**86**	**57**

Recruitment of patients included all those with lesions noted in the pelvic region in whole body planar images; this resulted in having a diverse variety of

diagnosis (about 32) in the study. The diagnoses frequencies in the sample were as shown in Table IV and illustrated Figure 19.

Table IV: Frequency Table of Diagnosis

Diagnosis	Frequency	Percent
Avascular Necrosis	9	8.55
Bunionectomy	1	0.95
Ca Breast	30	28.5
Ca Cervix	5	4.75
Ca Colon	2	1.9
Ca Nasopharyngeal	1	0.95
Ca of unknown Primary	2	1.9
Ca Ovary	1	0.95
Ca Prostate	18	17.14
Ca Rectum	2	1.9
Coccyx Pathology due to trauma	1	0.95
Fracture of the hip	2	1.9
Girdle stone on the left hip	1	0.95
Inflammation on the right hip joint	2	1.9
Mantle cell lymphoma	1	0.95
Multiple myeloma	1	0.95
Neuroendocrine tumour with bone metastases	1	0.95
Osteoarthritis hip	2	1.9
Osteodegenerative changes in SI joints	2	1.9
Osteomyelitis of the Hip	3	2.86
Osteosarcoma on the femur	2	1.9
Paget's disease on the left hip and pubis symphysis	1	0.95
Pain due to MVA	1	0.95
Pan uveitis Pseudo tumour, Retro orbital mass	1	0.95
Pathological Femur Fractures	3	2.86
Renal cell Carcinoma	1	0.95
Sacroiliatis	2	1.9
Septic arthritis of the hip joint	2	1.9
Severe Osteoarthritis and gout	1	0.95
Spondylosis with Lysthesis on L5 and S1	1	0.95
Stress fracture of the femur	2	1.9
Tronchanteric Bursitis	1	0.95
TOTAL	**105**	**100%**

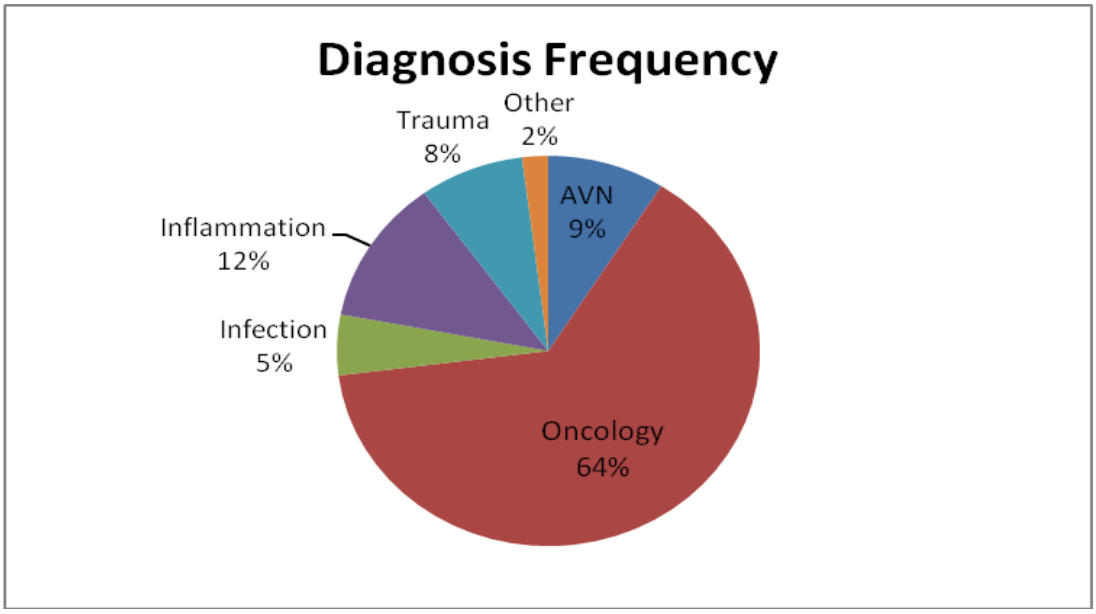

Fig. 19: Diagnosis of patients

As noted above Oncology-related referrals made up the majority of our study population (64%) with the high prevalent cancers being breast (45%) and prostate (27%). Inflammation, Avascular necrosis of the head of the femur (AVN) and trauma-related indications were the next most common reasons for referral (see Fig. 20).

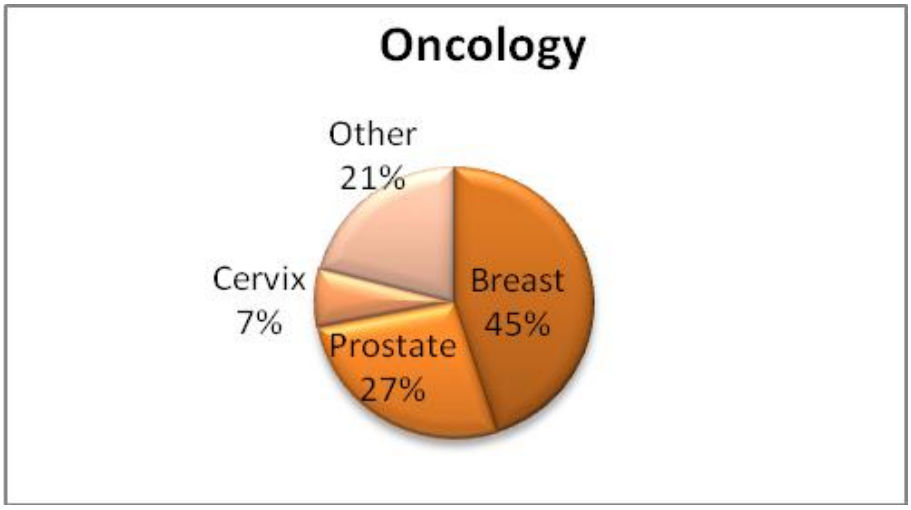

Fig. 20: Diagram showing percentagr of different malignancies in patient group

The Table below shows frequency of diagnoses in relation to gender.

Table V: Frequency Table of Diagnoses in Relation to Gender

Diagnosis	Gender		Total
	Female	Male	
Avascular Necrosis	5	4	9
Bunionectomy	0	1	1
Ca Breast	30	0	30
Ca Cervix	5	0	5
Ca Colon	1	1	2
Ca Nasopharyngeal	0	1	1
Ca of unknown Primary	2	0	2
Ca Ovary	1	0	1
Ca Prostate	0	18	18
Ca Rectum	1	1	2
Coccyx Pathology due to trauma	1	0	1
Fracture of the hip	1	1	2
Girdle stone on the left hip	0	1	1
Inflammation on the right hip joint	2	0	2
Mantle cell lymphoma	0	1	1
Multiple myeloma	0	1	1
Neuroendocrine tumour with bone metastasis	0	1	1
Osteoarthritis hip	1	1	2
Osteodegenerative changes in SI joints	1	1	2
Osteomyelitis of the Hip	0	3	3
Osteosarcoma on the femur	0	2	2
Paget's disease on the left hip and pubis symphysis	1	0	1
Pain due to MVA	0	1	1
Pan uveitis Pseudo tumour, Retro orbital mass	0	1	1
Pathological Femur Fractures	2	1	3
Renal cell Carcinoma	0	1	1
Sacroiliatis	2	0	2
Septic arthritis of the hip joint	0	2	2
Severe Osteoarthritis and gout	0	1	1
Spondylosis with Lysthesis on L5 and S1	0	1	1
Stress fracture of the femur	1	1	2
Tronchanteric Bursitis and right hip joint	1	0	1

With the 30 subjects found with Breast cancer, 22 were observed to be in the 36 – 75 years age bracket (Table VI), while no subjects had Prostate cancer below 55 in the sample (Table VII).

Table VI: Diagnosis Ca Breast

Diagnosis	< 35 years	36 – 55 years	56 – 75 years	>76 years	**Total**
Ca Breast	3	10	12	5	30
Total	3	10	12	5	30

Table VII: Diagnosis Ca Prostate

Diagnosis	56 – 75 years	Over 76 years	**Total**
Ca Prostate	15	3	18
Total	15	3	18

As stated previously, three different human observers (three nuclear medicine physicians) took part in this study to evaluate lesion detectability on images reconstructed with OSEM over those reconstructed with FBP subjectively and rated on the 4- point scale, where Grade 1 corresponded to Non-diagnostic image, Grade 2 to Poor quality image (Lesion/Background ratio <1), Grade 3 to Adequate quality image (Lesion/Background ratio = 1), and Grade 4 to Good quality image (Lesion/Background ratio >1).

Each observer was shown a set of 105 images each. Each set consisted of two images, one reconstructed using FBP method of reconstruction, and the second one reconstructed using OSEM iterative method of reconstruction. The observer, blind to either the type of data reconstruction used or the subset-iteration combination, was then asked to rate the images to the 4- point scale.

It was observed that out of the 105 images reconstructed using FBP reconstruction method, only 13 images were rated as good quality images in comparison to those which were reconstructed using OSEM reconstruction method (Table VIII).

Table VIII: FBP Frequency

FBP	Frequency	Percent	Cumulative
1	13	100.0	100.0
Total	13	100.0	

In contrary, out of 105 images reconstructed using OSEM method of reconstruction 92 images were rated to as good quality images in comparison to the ones reconstructed using FBP method of reconstruction (Table IX and Fig. 21).

Table IX: OSEM Frequency

OSEM	Frequency	Percent	Cumulative
1	92	100.0	100.0
Total	92	100.0	

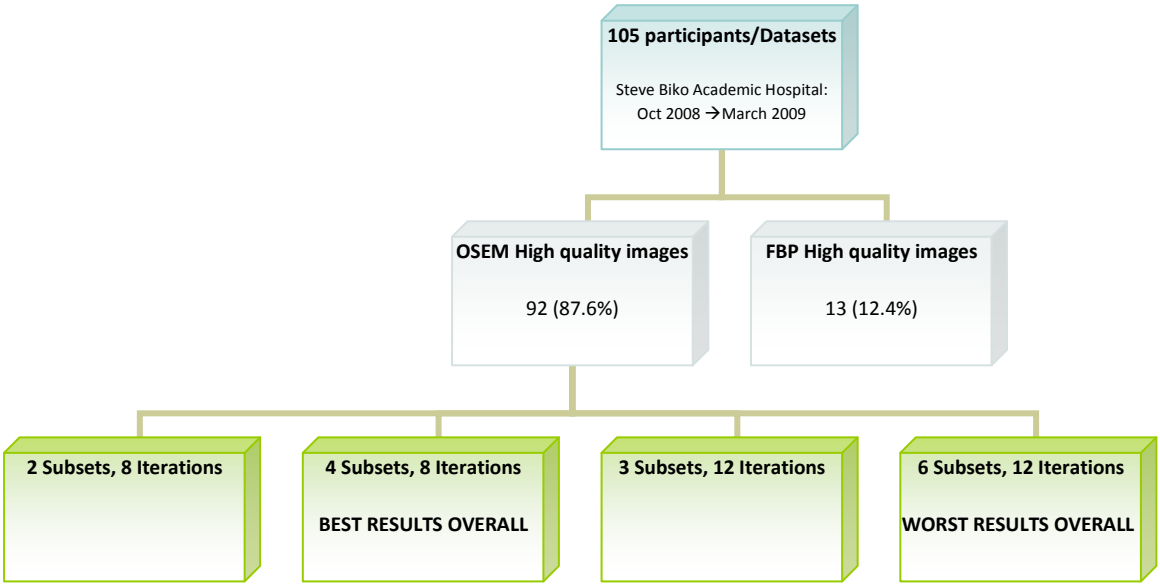

Fig. 21

It was further demonstrated that the (subset x iterations) used for reconstruction of an image correlates with the (A/B) ratio. (4 x 8) yielded the best results in **48.5%** of the images whilst (2 x 8) yielded the best results in **33.8%.** The number of reconstructed images which yielded the best results with (2 x 8) was the same as or more than those with (4 x 8) when the (A/B) ratio was between 0.20-0.39. A ratio below 0.20 or above 0.39 supported the use of (4 x 8) over (2 x 8). Although it is less common, should the ratio be

above 0.69, then (3 x12) will provide image qualities of grade 3 & 4 (See Results Graph, Fig 22).

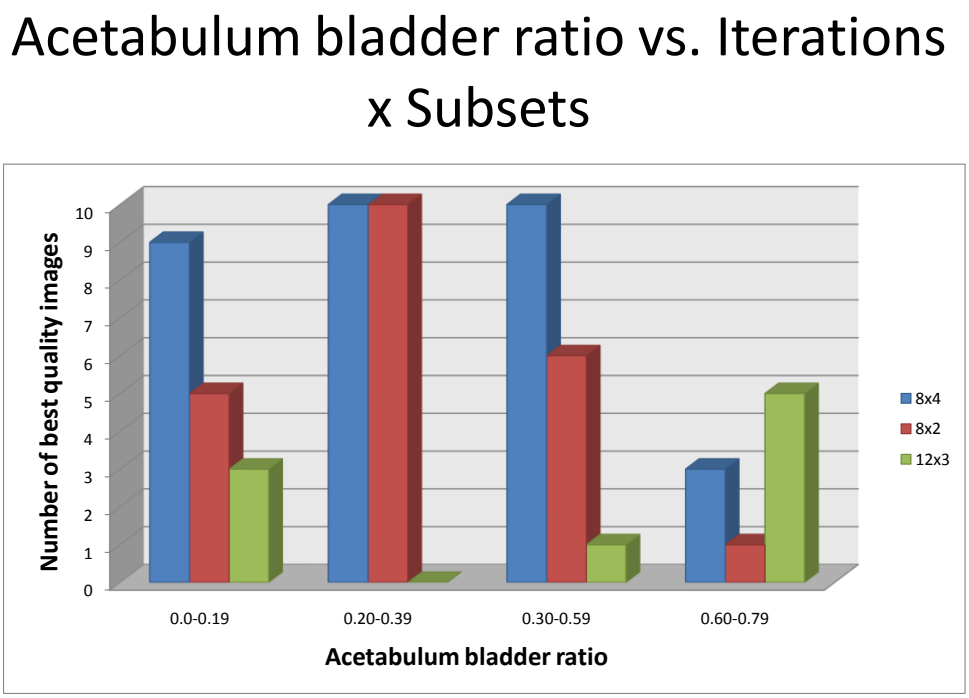

Fig. 22

Using sign testor by Kruskaal – Wallis for comparing the population, it was established that the two methods of reconstruction are significantly different ($p = 1.000$, $p = 0.000$).

As noted from the results, in all reconstructed images OSEM reconstruction method led to a significant reduction in bladder artifacts when compared to FBP reconstruction method (Table X).

Table X: Frequency of Reconstruction Methods

Reconstruction Method	Observation	Percentage
1. OSEM	92	87.62
2. FBP	13	12.38
Total	**105**	**100.00**

Kruskaal Wallis Statistical method of analysis was used in this study. It is a non-parametric method for testing equality of population medians among groups. Intuitively, it is identical to a one-way analysis of variance with the data replaced by their ranks.

Table XI: Kruskal-Wallis Equality of populations Rank Test

Reconstruction Method	Observation	Rank Sum
1. OSEM	92	5474.00
2. FBP	13	91.00

Chi-squared with ties = 104.000 with 1 d.f.

Probability = 0.0001

Table XI implies that images reconstructed using FBP method of reconstruction completely differs from images reconstructed using OSEM method of reconstruction.

The results showed that, compared with FBP (p = 0.000), OSEM method of reconstruction significantly reduced (p = 1.000) the bladder artifact in the pelvis in SPECT imaging, it improved the uniformity and symmetry of bone tracer-uptake, and thus optimizing lesion detectability. The reduction of pelvic bladder artifacts in the OSEM reconstructed images was independent of diagnosis, age or gender of the patients.

It was also noted that, in situations where images reconstructed by FBP method of reconstruction provided accurate lesion detectability and localization, OSEM reconstructed images could not improve more.

CHAPTER 5

DISCUSSION

In this study, it was found that OSEM show a clear advantage in the quality of the reconstructed image, but there is understandably a concern over the price paid in reconstruction time which may introduce delays into the daily work flow. This can be overcome by either installation of faster hardware, or by using large subset size (between 4 and 8) to speed up the reconstruction [46] and hence spare time.

It was also noted that for most patient with acetabulum bladder hip ratio of less than 0.6 (8 iterations and 4 subsets) provided the best images whilst above that 0.6 (12 iterations x 3) subset provides the best images Fig 23.

Bladder artifacts in pelvic SPECT are known to be caused by the nonuniform attenuating media and changing bladder activity [47], both of which also lead to incomplete cancellation of side lobes in FBP, and so iterative reconstruction would be expected to reduce the magnitude of the artifact.

With the availability of faster hardware and more efficient iterative reconstruction techniques, algorithms such as OSEM are now moving from the research environment into routine clinical use. It is important to understand

the quality control requirements that such algorithms place on the imaging system. These requirements are well known for FBP, and some work is to be done to determine the uniformity requirements for algorithms such as OSEM. Though it has been reported previously that, in clinical practise, the use of iterative reconstruction techniques in place of FBP does not appear to alter the basic requirements for good gamma camera uniformity, as the uniformity requirements for SPECT are not significantly influenced by the reconstruction technique, but the accuracy and validity of this information has not been critically examined as the results were limited on data obtained using subset size of 1 while number of iterations was set at 40 (in OSEM reconstruction method) [46]. The current study either, did not critically analyse the uniformity requirements for the reconstructed methods used having fixed the pixel size and the amount of post reconstruction filtering.

Despite diversity of diagnosis, images reconstructed with OSEM method of reconstruction showed the best reduction of pelvic bladder artifacts, irrespective of the age or gender of the patients, when compared to images reconstructed with FBP method of reconstruction. But in cases where avascular necrosis of the head of femur is suspected, very high resolution planar images of the region, acquired using pinhole collimator have advantage over SPECT pelvic images reconstructed with OSEM method of

reconstruction[48]. In some cases, a simple additional delayed (6 – 24hrs) planar image may result in higher target to background ratio, and permit better evaluation of the pelvis if it was obscured by the bladder, thus excluding the need for pelvic SPECT imaging. Hence, the results obtained are bound in comparing FBP and OSEM method of reconstruction in reducing bladder artifacts, when SPECT pelvic imaging is necessary for accurate localization and detection of lesion.

The use of the acetabulum bladder ratio provides an individualized ratio for which the most appropriate number of iterations and subset may be chosen.

LIMITATIONS

This study was limited to comparison of FBP and OSEM only (one among variable iterative method of reconstruction) in reducing bladder artifacts in SPECT pelvic imaging. The two are the only working methods of reconstruction programmed in the processing computers in the department.

Limited number of subsets programmed (nine different subsets) and number of iterations (limited to 30) in the OSEM reconstruction, was another limitation encountered during reconstructions. It has been observed that, for OSEM with a subset size of 1, the number of iterations required to achieve good image quality is above 30 [39]. This means, different subset sizes appear to have

significant effect on reconstructed images when an adequate number of iterations are not performed [37].

This study did perfectly model the clinical situation, and mirror the variability and complexity of true patient backgrounds. Hence these results can be directly applicable to our department. They are an encouraging indication that OSEM reduces bladder artifacts, and hence improve diagnostic performance over FBP for detecting and accurately localization of lesions in pelvic SPECT imaging.

The number of iterations and subsets chosen depend on a number of factors including the dose of tracer injected, the pixel size and other camera parameters so it is important that the best images and ratios are determined for each Nuclear Medicine department.

CHAPTER 6

CONCLUSION

In this research we have defined the effect of OSEM reconstruction and, its impact versus filtered back projection in reducing bladder artifacts in pelvic SPECT imaging. It has been proved that, OSEM iterative reconstruction performs significantly better than FBP. The bladder-filling artifact was significantly reduced in most patients. Subjective evaluation of image quality did demonstrate a significant difference between OSEM and FBP. The reduction of pelvic bladder streak artifacts in the OSEM reconstructed images was independent of diagnosis, age or gender of the patients.

OSEM improved diagnostic performance over FBP reconstructed images for accurately detecting and localizing lesions, after reducing bladder artifacts in pelvic SPECT imaging.

The study also demonstrates that the acetabulum bladder ratio is a good index to determine the number of iterations and subsets to be chosen for reconstruction of pelvic SPECT by OSEM.

REFERENCES

1. Collier B, Carrera G, Johnson R, et al. Detection of femoral head avascular necrosis in adults by SPECT. J Nucl Med. 1985;26:979–987
2. King MA, Tsui BMW, Pan TS, Glick SJ, Soares EJ. Attenuation compensation for cardiac single-photon emission computed tomographic imaging: Part 2. Attenuation compensation algorithms. J Nucl Cardiol. 1996;3:55–63
3. Wells RG, King MA, Simkin PH, et al. Comparing FBP and OSEM for small lesion detection and localization in Ga-67 SPECT. J Nucl Med. 2000; 41:1391–1399.
4. Gillen G, McKillop J, Hilditch T, Davidson J, Elliot A. Digital filtering of the bladder in SPECT bone studies of the pelvis. J Nucl Med. 1988; 29:1587–1595.
5. Case J, Licho R, King M, Weaver J. Bone SPECT of the spine: a comparison of attenuation correction techniques. J Nucl Med. 1999;40:604–613
6. Licho R, Wells RG, King MA. Evaluation of non-uniform attenuation- and scatter-correction in bone SPECT of the cervical, thoracic, and lumbar spine [abstract]. J Nucl Med.2000;41(suppl):328P
7. Turkington T, Coleman R. Effects of reconstruction methods and attenuation correction on hot bladder artifacts in PET [abstract]. J Nucl Med. 2000; 41(suppl):194P.
8. Bunker S, Handmaker H, Torre D, Schmidt W. Pixel overflow artifacts in SPECT evaluation of the skeleton. Radiology. 1990;174:229–232
9. O'Connor M, Kelly B. Evaluation of techniques for the elimination of "hot" bladder artifacts in SPECT of the pelvis. J Nucl Med. 1990;31:1872–1875
10. Penney B, Al-Hallaq H, Keast R, Ryan J. Summing rapid SPECT acquisitions reduces bladder filling artifact [abstract]. J Nucl Med. 1996; 37(suppl):212P.
11. Gillen GJ, Gilmore B, Elliott AT. An investigation of the magnitude and causes of count loss artifacts in SPECT imaging. J Nucl Med 1991; 32:1771.–1776.

12. Forstrom LA, Dunn WL, O'Connor MK, et al. Technical pitfalls in image acquisition, processing and display. Semin Nucl Med 1996; 26:278. –294.

13. Hutton BF, Hudson HM, Beekman FJ. A clinical perspective of accelerated statistical reconstruction. Eur J Nucl Med 1997; 24:797. –808

14. Udson HM, Larkin RS. Accelerated image reconstruction using ordered subsets of projection data. IEEE Trans Med Imaging 1994; 13:601–609.

15. Locklet D, Seret A, Popa N, et al. Maximum-likelihood reconstruction with ordered subsets in bone SPECT. J Nucl Med 1999; 40:1978. –84.

16. Alush DS, Tsui BM. Performance of ordered-subset reconstruction algorithms under conditions of extreme attenuation and truncation in myocardial SPECT. J Nucl Med 2000; 41:737. –44

17. Gardner RJ. *Geometric Tomography*. Cambridge University Press, Cambridge, 1995

18. Jain AK. Fundamentals of Digital Image Processing. Prentice-Hall, 1989

19. English RJ. SPECT Single Photon Emission Tomography: A Primer. Society of Nuclear Medicine, 1995

20. Connor MK, Vermeersch C. Critical examination of the uniformity requirements for single-photon emission computed tomography. Med Phys 1991; 18:190. –197.

21. llberg GT. An analytical approach to quantify uniformity artifacts for circular and noncircular detector motion in single photon emission computed tomography imaging. Med Phys 1987; 14:105.–114.

22. Wilson DW, Tsui BMW. Noise properties of filtered-back projection and ML-EM reconstructed emission tomographic images. IEEE Trans Nucl Sci 1993; 40:119. 8. –1203

23. Collier B, Carrera G, Johnson R, et al. Detection of femoral head avascular necrosis in adults by SPECT. J Nucl Med. 1985; 26:979–987.

24. Ing MA, Tsui BMW, Pan TS, Glick SJ, Soares EJ. Attenuation compensation for cardiac single-photon emission computed tomographic imaging: Part 2. Attenuation compensation algorithms. J Nucl Cardiol. 1996; 3:55–63.

25. Blocklet D, Seret A, Popa N, Schoutens A, Maximum likelihood reconstruction with ordered subsets in bone SPECT. J Nucl Med 1999; 40: 1978 – 1984

26. Case JA, Licho K, King MA, Weaver JP, Bone SPECT of the spine: a comparison of attenuation correction techniques. J Nucl Med 1999, 40: 604 – 613

27. Kauppinen T, Koskinen MO, Alenius S, Vanninen E, Kuikka JT, Improvement of brain perfusion SPET using iterative reconstruction with scatter and non – uniform attenuation correction, Eur J Nucl Med 2000, 27: 1380 – 1386

28. Vanhove C, Defrise M, Frankers PR, Evernert H, Deconinck F, Bossyut A, Interest of the ordered subsets expectation maximization (OSEM) algorithm in pinhole single-photon emission tomography reconstruction: a phantom study. Eur J Nucl Med 2000, 27: 140 – 146.

29. Wells GR, King MA, Simkin PH, Judy PF, Brill AB, Gifford HC et al. comparing filtered back projection and ordered subsets expectation maximization for small- lesions detection and localization in 67Ga SPECT. J Nucl Med 2000, 41: 1391 – 1399.

30. Blocklet D, Seret A, Popa N, Schoutens A. Maximum likelihood reconstruction with ordered subsets in bone SPECT. *J Nucl Med* 1999; 40: 1978–1984.

31. Case JA, Licho R, King MA, Weaver JP. Bone SPECT of the spine: a comparison of attenuation correction techniques. *J Nucl Med* 1999; 40: 604–613.

32. Kauppinen T, Koskinen MO, Alenius S, Vanninen E, Kuikka JT. Improvement of brain perfusion SPET using iterative reconstruction with scatter and non-uniform attenuation correction. *Eur J Nucl Med* 2000; 27: 1380–1386.

33. Vanhove C, Defrise M, Franken PR, Everaert H, Deconinck F, Bossuyt A. Interest of the ordered subsets expectation maximization (OS-EM) algorithm in pinhole single-photon emission tomography reconstruction: a phantom study. *Eur J Nucl Med* 2000; 27: 140–146.

34. Wells GR, King MA, Simkin PH, Judy PF, Brill AB, Gifford HC, et al. Comparing filtered backprojection and ordered subsets expectation maximization for small-lesions detection and localization in 67Ga SPECT. *J Nucl Med* 2000; 41: 1391–1399.

35. Van der Weerdt AP, Boellaard R, Knaapen P, Visser CA, Lammertsma AA, Visser FC. Postinjection transmission scanning in myocardial 18F-FDG PET studies using both filtered back projection and iterative reconstruction. *J Nucl Med.* 2004; 45:169–175.

36. Boellaard R, van Lingen A, Lammertsma AA. Experimental and clinical evaluation of iterative reconstruction (OSEM) in dynamic PET: quantitative characteristics and effects on kinetic modeling. *J Nucl Med.* 2001; 42:808–817.

37. Mesina CT, Boellaard R, Jongbloed G, et al. Experimental evaluation of iterative reconstruction versus filtered back projection for 3D [15O] water PET activation studies using statistical parametric mapping analysis. *Neuro image.* 2003; 19:1170–1179.

38. Boellaard R, Kropholler MA, de Jong HWAM, Lammertsma AA. Evaluation of iterative reconstruction algorithms for reconstruction of 3D PET brain studies. *J Cereb Blood Flow Metab* [abstract]. 2003; 23(suppl 1): 610.

39. Chen GP, Branch KR, Alessio AM, Pham P, Tabibiazar R, Kinahan P, and Caldwell JH. Effect of Reconstruction Algorithms on Myocardial Blood Flow Measurement with 13N-Ammonia PET J. Nucl. Med., August 1, 2007; 48(8): 1259 - 1265.

40. Jaskowiak CJ, Bianco JA, Perlman SB, and Fine JP. Influence of Reconstruction Iterations on 18F-FDG PET/CT Standardized Uptake Values J. Nucl. Med., March 1, 2005; 46(3): 424 - 428.

41. Bouchareb, K. Thielemans, T. Spinks, O. Rimoldi and P.G. Camici, Comparison of analytic and iterative reconstruction methods for quantitative cardiac PET studies in 3D using Oxygen-15 water scans, IEEE Nucl. Sci. Symp. Conf. Rec. 4 (2005), pp. 2120–2123.

42. Lartizien C, Kinahan PE, Swensson R, Comtat C, Lin M, Villemagne V and Trébossen R, Evaluating image reconstruction methods for tumor detection in 3-dimensional whole-body PET oncology imaging, J. Nucl. Med. 4 (2) (2003), pp. 276–290 (Feb.).

43. Gutman F, Gardin I, Delahaye N, Rakotonirina H, Hitzel A, Manrique A, Guludec DL and Véra P. Optimisation of the OS-EM algorithm and comparison with FBP for image reconstruction on a dual-head camera: a phantom and a clinical ^{18}F-FDG study, Eur. J. Nucl. Med. Mol. Imaging 30 (11) (2003), pp. 1510–1519 (Nov.)

44. Reilhac A, Tomeï S, Buvat I, Michel C, Keheren F, Costes N. Simulation-based evaluation of OSEM iterative reconstruction methods in dynamic brain PET studies. Neuro image. 2008 Jan 1; 39(1):359-68.

45. Leong LK, Kruger RL, O'Connor MK. A Comparison of the Uniformity Requirements for SPECT Image Reconstruction Using FBP and OSEM Techniques. J Nucl Med Technol 2001; 29:79-83

46. Gillen G, Gilmore B, Elliot A. An investigation of the magnitude and causes of count loss artifacts in SPECT imaging. J Nucl Med. 1991;32:1771–1776

47. Hudson HM, Larkin RS. Accelerated image reconstruction using ordered subsets of projection data. IEEE Trans Med Imaging 1994; 13:601.–609

48. Hofman S, Staudennkerg A, Breitenseker M, et al. Diagnostic patterns for bone marrow edema syndrome and avascular necrosis of the femoral head in dynamic bone scintigraphy. *Nucl Med Commentary*. 1997;18 (12):1178.